

ESCUELA TÉCNICA SUPERIOR DE INGENIEROS
INDUSTRIALES Y DE TELECOMUNICACIÓN

UNIVERSIDAD DE CANTABRIA



Trabajo Fin de Grado

**Diseño y puesta a punto de un biorreactor
de perfusión con membranas como soporte
celular para ingeniería tisular: análisis
experimental y modelado**

**(Design and tune up of a perfusion bioreactor
with membranes as scaffolds for tissue
engineering: experimental assessment and
modelling)**

Para acceder al Título de

Graduada en Ingeniería Química

Autor: María de los Ángeles Mantecón Oria

Julio – 2018

INDEX

1. APPROACH	1
1.1. TISSUE ENGINEERING	2
1.2. TISSUE ENGINEERING BIOREACTORS	3
1.2.1. Perfusion Bioreactor	4
1.3. OVERVIEW OF MATHEMATICAL MODELS DESCRIBING MASS TRANSPORT OF NUTRIENTS IN PERFUSION BIOREACTORS FOR TE.....	6
1.4. OBJECTIVES	8
2. DEVELOPMENT.....	9
2.1. EXPERIMENTAL SETUP	10
2.2. MEMBRANE CHARACTERIZACION	13
2.2.1. Membrane thickness	13
2.2.2. Water flux membrane characterization	13
2.2.3. Glucose diffusivity in PCL/rGO scaffold	13
2.3. BIOREACTOR FLUX EXPERIMENTS	14
2.3.1. Oxygen sensing system calibration	14
2.3.2. Water experiments	16
2.3.3. BSA+Glucose model solution filtration tests	17
2.4. MODELLING WITH ASPEN CUSTOM MODELER	18
3. RESULTS AND DISCUSSION.....	24
3.1. MEMBRANE CHARACTERIZATION.....	25
3.1.1. Glucose diffusion coefficient.....	26
3.2. OXYGEN SENSING SYSTEM RESULTS	28
3.3. EXPERIMENTAL SETUP DATA	30
3.4. MATHEMATICAL MODEL RESULTS	36
3.4.1. Analysis of parameters sensitivity	36
4. CONCLUSIONS AND FUTURE CHALLENGES	40
5. REFERENCES	43
6. APPENDIX	48
Appendix A: Peristaltic Pump Calibration	49
Appendix B: Cross-flow filtration setup	49
Appendix C: Glucose and lactate quantification protocols	50
Appendix D: Dynamic cell culture.....	51
Appendix E: Mathematical model development	54
Appendix F: Glucose diffusivity results.....	66

Appendix G: Continuous and discrete measurements of oxygen.....	69
Appendix H: Reynolds number calculation	69
Appendix I: Cells growth kinetic parameters.....	70

INDEX OF TABLES

Table 1. 1. Different tissue engineering bioreactors [5], [6].....	5
Table 2. 1. Experiments done with the oximeter at 37 °C.....	15
Table 2. 2. PBS composition.....	18
Table 2. 3. Empirical dead-end filtration equations [21]	20
Table 2. 4. Parameter values used in simulations	22
Table 2. 5. Operating conditions.....	22
Table 3. 1. Comparison of the hydraulic permeances of the PCL and PCL-graphene membranes with other polymer membranes reported in the literature	26
Table 3. 2. Comparison of effective diffusion coefficients for glucose across typical TE scaffolds saturated in water.....	28
Table 3. 3. Fouling mechanisms adjustment	31
Table 6. 1. Average data for glucose diffusivity experiments.....	67
Table 6. 2. Data for calculated the Re number in the perfusion cell.	69

INDEX OF FIGURES

Figure 1. 1. Schematic diagram of tissue engineering principle using flat sheet polymeric membranes as scaffolds and tangential diffusion perfusion bioreactor	3
Figure 2. 1. Experimental setup	10
Figure 2. 2. A) Vascular chamber, B) Cellular chamber, C) Top piece and D) Perfusion cell assembled	10
Figure 2. 3. Diffusion cell with glucose and ultrapure water compartments, connecting by the membrane.....	14
Figure 2. 4. Sensing spot layers.....	15
Figure 2. 5. A) Oxygen sensor and alimentation tank with spot, b) oxygen device + perfusion cell	16
Figure 3. 1. Clean water flux for PCL/rGO at different transmembrane pressures.....	25
Figure 3. 2. Evolution of glucose concentration with time of diffusion cell experiments in PCL/rGO scaffolds at room temperature	26
Figure 3.3. Oxygen concentration in water for tap water, distilled water and UP water, with and without recirculation.....	29
Figure 3. 4. Total permeate flux for experiments at different inlet flowrates (zoom).	30
Figure 3. 5. Experimental data at different feed flowrates (1 and 8.5 mL min ⁻¹) fitted with the different models proposed	33
Figure 3. 6. Progression of permeate flowrate with time for experimental data and model developed.....	34
Figure 3. 7. Evolution of the protein transmission with time.	35
Figure 3. 8. Evolution of the glucose transmission with time.....	35

Figure 3. 9. Variation of glucose concentration in cellular chamber for different initial culture medium volume	37
Figure 3. 10. Variation of lactate concentration in cellular chamber for different initial culture medium volume	38
Figure 3. 11. Variation of oxygen concentration in cellular chamber for different initial culture medium volume	38
Figure 6. 1. Calibration line of the Peristaltic Pump-MINIPULS 3	49
Figure 6. 2. Homemade cross-flow filtration system.....	49
Figure 6. 3. Calibration line of glucose concentration from absorbance UV	50
Figure 6. 4. Total permeate flux during the dynamic experiment	53
Figure 6. 5. Confocal microscopy images of the dynamic cell culture of the U87 cells on the PCL/rGO membranes at (a) 3 h and (b) 7 days.....	53
Figure 6. 6. ACM diagram for the perfusion BR system.....	59
Figure 6. 7. Variation of the concentration gradient with time.....	68
Figure 6. 8. Glucose diffusion flux versus concentration gradient	68
Figure 6. 9. Oxygen concentration with and without recirculation, for continuous and discrete measurements in water	69
Figure 6. 10. Variation of glucose concentration with time depending on the maintenance coefficient.....	70
Figure 6. 11. Variation of lactate concentration with time depending on the maintenance coefficient.....	71
Figure 6. 12. Variation of lactate concentration with time depending on the Yps yield coefficient.....	71
Figure 6. 13. Variation of glucose concentration with time depending on the Yxs yield coefficient.....	72
Figure 6. 14. Variation of lactate concentration with time depending on the Yxs yield coefficient.....	72

TÍTULO	Diseño y puesta a punto de un biorreactor de perfusión con membranas como soporte celular para ingeniería tisular: análisis experimental y modelado		
AUTOR	María de los Ángeles Mantecón Oria		
DIRECTOR/CODIRECTOR	Nazely Diban-Ibrahim Gómez/Sandra Sánchez González		
TITULACIÓN	<i>Grado en Ingeniería Química</i>	FECHA	Julio 2018

PALABRAS CLAVE

Ingeniería de tejidos, membranas poliméricas biocompatibles: PCL/rGO, scaffolds, fouling, biorreactor de perfusión, proliferación y diferenciación de células neuronales, modelado, estimación paramétrica y análisis de sensibilidad

PLANTEAMIENTO DEL PROBLEMA

Conseguir regenerar tejido del Sistema Nervioso Central (SNC) in vitro para su uso como modelo neuronal supondría un avance de suma importancia para el diagnóstico, comprensión y tratamiento de enfermedades tanto traumáticas como neurodegenerativas; sin embargo, supone uno de los retos más ambiciosos para la Ingeniería Tisular [1]. La propuesta tiene como punto de partida nuevas membranas funcionalizadas fabricadas a partir de conjugar materiales poliméricos biocompatibles, la policaprolactona (PCL) con grafeno y sus derivados para producir nuevos materiales compuestos con elevadas propiedades electro-conductivas que estimulen la diferenciación reproducible de células madre en células neuronales para, posteriormente, incorporarlos en sistemas de cultivo in vitro [8].

El proyecto se centra en el diseño y montaje de un biorreactor de perfusión que incorpore estas membranas para la consecución de tejido neuronal como preludeo para demostrar su potencialidad para ser usado en modelos neuronales que presenten funcionalidad sináptica cerebral.

RESULTADOS

El presente trabajo ha cumplido con el diseño y montaje del sistema del biorreactor de perfusión, así como con la puesta a punto del mismo en condiciones hidrodinámicas simuladas de cultivo celular. El sistema de biorreactor de perfusión incluye: 1) celda de perfusión que incorpora una cámara vascular y otra de cultivo celular, 2) tanque de alimentación de medio de cultivo, 3) bomba peristáltica para simular bombeo por impulsos del medio de cultivo a la cámara vascular, 4) oxímetro para monitorizar en continuo la concentración del nutriente oxígeno en la cámara de cultivo celular y 5) transductor de presión para monitorizar la presión tras-membrana que se ejerce en la celda de perfusión y que controla el flujo constante de nutrientes desde la cámara vascular a la cámara celular. Se ha conseguido la calibración del medidor de oxígeno, eliminando fugas del sistema, logrando el menor volumen muerto posible, etc.

El sistema se ha probado tanto en agua ultrapura como en una disolución modelo de Suero de Albumina Bovina (BSA) y glucosa disueltos en una disolución buffer de fosfato (PBS) a pH 7.2 en condiciones simuladas de cultivo celular a 37°C. Los ensayos de perfusión se han llevado a cabo durante 3 días y han sido replicados. Además, se han monitorizado los resultados de flujo total y transmitancia de los nutrientes modelo BSA y glucosa a través de la membrana, necesarios para garantizar la alimentación de las células soportadas en la membrana.

Finalmente se ha desarrollado un modelo en Aspen Custom Modeler que tiene en cuenta el fenómeno de ensuciamiento por deposición de proteínas BSA en las membranas de microfiltración y los parámetros de crecimiento celular de acuerdo a un modelo cinético de Monod. Con ello se ha completado la toma de decisión de variables del proceso permitiendo un estudio más adecuado. Además, se ha llevado a cabo un análisis de sensibilidad para la variable de volumen de medio de cultivo y otro, teniendo en cuenta la influencia de los parámetros de crecimiento celular para futuros estudios de cultivo de células neuronales en dinámico con el sistema del biorreactor de perfusión.

CONCLUSIONES

Se han analizado los mecanismos de fouling usuales para la membrana de PCL/rGO ajustando los datos experimentales obtenidos a los modelos desarrollados. Se ha visto que un modelo combinado que tiene en cuenta el bloqueo de los poros debido a la adsorción de la proteína BSA y la formación de una torta sobre la superficie de la membrana puede predecir correctamente el fenómeno de fouling en las membranas.

La calibración y los experimentos desarrollados con el medidor de oxígeno, así como el modelo matemático desarrollado en ACM han permitido determinar que el oxígeno no es un nutriente crítico en este sistema. Además, el modelo matemático ha servido para demostrar la viabilidad del cultivo de diferentes sistemas celulares en el sistema del biorreactor de perfusión prediciendo la variación de la concentración de glucosa, lactato y oxígeno en el sistema.

Con este proyecto se ha conseguido avanzar hacia el objetivo de conseguir desarrollar un modelo neuronal en el sistema del biorreactor de perfusión con el uso de membranas biocompatibles y biodegradables de PCL/rGO.

BIBLIOGRAFÍA

- [1]. IKADA, Y. 2006. Challenges in tissue engineering. *Journal of the Royal Society Interface*, **3** (10), pp. 589-601. ISSN: 1742-5689.
- [8]. DIBAN, N. [et al.]. 2017. Facile fabrication of poly (ϵ -caprolactone)/graphene oxide membranes for bioreactors in tissue engineering. *Journal of Membrane Science*, **540**, pp. 219-228.

TÍTULO	Design and tune up of a perfusion bioreactor with membranes as scaffolds for tissue engineering: experimental assessment and modelling		
AUTOR	María de los Ángeles Mantecón Oria		
DIRECTOR/CODIRECTOR	Nazely Diban-Ibrahim Gómez/Sandra Sánchez González		
TITULACIÓN	<i>Grado en Ingeniería Química</i>	FECHA	Julio 2018

KEYWORDS

Tissue Engineering, biocompatible polymeric membranes: PCL/rGO, scaffolds, fouling, perfusion bioreactor, neural cell proliferation and differentiation, modelling, parametric estimation and sensitivity analysis

SCOPE

Achieving regeneration of tissue from the Central Nervous System (CNS) in vitro for use as a neuronal model would be an extremely important advance for the diagnosis, understanding and treatment of both traumatic and neurodegenerative diseases; however, it is one of the most ambitious challenges for Tissue Engineering [1].

The proposal has as starting point new functionalized membranes manufactured from conjugate biocompatible polymeric materials, polycaprolactone (PCL) with graphene and its derivatives to produce new composite materials with high electro-conductive properties that stimulate the reproducible differentiation of stem cells into neuronal cells to subsequently incorporate them into in vitro culture systems [8].

The project focuses on the design and assembly of a perfusion bioreactor that incorporates these membranes for the achievement of neuronal tissue as a prelude to demonstrate its potential to be used in neuronal models that present cerebral synaptic functionality.

RESULTS

The present work has complied with the design and assembly of the perfusion bioreactor system, as well as the set-up of the same in simulated hydrodynamic conditions of cell culture. The perfusion bioreactor system includes: 1) perfusion cell that incorporates a vascular and cell culture chamber, 2) culture medium feed tank, 3) peristaltic pump to simulate pumping impulse of the culture medium to the vascular chamber, 4) oximeter to continuously monitoring the concentration of the oxygen nutrient in the cell culture chamber and 5) pressure transducer to monitor the transmembrane pressure that is exerted in the perfusion cell and that controls the constant flow of nutrients from the vascular to the cell chamber. The calibration of the oximeter has been achieved, eliminating leaks in the system, achieving the lowest possible dead volume, etc.

The system has been tested in both ultrapure water and in a model solution of Bovine Albumin Serum (BSA) and glucose dissolved in a phosphate buffer solution (PBS) at pH 7.2 under simulated cell culture conditions at 37 °C. Perfusion tests have been carried out for 3 days and have been replicated. In addition, the results of total flow and transmittance of the BSA model and glucose nutrients through the membrane, necessary to guarantee the feeding of the cells supported in the membrane, have been monitored.

Finally, a model has been developed in Aspen Custom Modeler that takes into account the phenomenon of fouling by protein BSA deposition in microfiltration membranes and cell growth parameters according to a kinetic model of Monod. With this, decision making of process variables has been completed to allow a more adequate experimental study. In addition, a sensitivity analysis was carried out taking into account the culture medium volume and the influence of cell growth parameters for future culture cell studies of neuronal cells in dynamic with the perfusion bioreactor system.

CONCLUSIONS

The fouling mechanisms phenomena in the biocompatible and biodegradable PCL/rGO membrane has been analyzed adjusting the experimental data to the models. It has been seen that a combined model of pore blockage that takes into account the adsorption of BSA protein in the pores and cake filtration can correctly predict the phenomenon of fouling in the scaffolds.

The calibration and experimentation of the oximeter, as well as the mathematical model developed in ACM, allowed determine that the O₂ is not a critical nutrient in this system. In addition, the mathematical model has served to demonstrate the feasibility of growing different cellular types in perfusion bioreactor system predicting the variation of the most important variables.

With this project, it has been possible to progress towards the objective of developing a neuronal model in the perfusion bioreactor system with the use of biocompatible and biodegradable membranes of PCL/rGO.

REFERENCES

- [1]. IKADA, Y. 2006. Challenges in tissue engineering. *Journal of the Royal Society Interface*, **3** (10), pp. 589-601. ISSN: 1742-5689.
- [8]. DIBAN, N. [et al.]. 2017. Facile fabrication of poly (ε-caprolactone)/graphene oxide membranes for bioreactors in tissue engineering. *Journal of Membrane Science*, **540**, pp. 219-228.

1. APPROACH

1.1. TISSUE ENGINEERING

The total or partial damaged tissues and the failure of organs represent one of the most expensive and serious problems of current medicine. Traditionally such problems have been mitigated with the transplantation of organs and tissues. The indicated is an efficient option but it is limited by the low availability of donors and the high risk of incompatibility. For these reasons, a new field has emerged, tissue engineering (TE).

TE is the branch of regenerative medicine that makes use of porous scaffolds to act as support for cell proliferation, differentiation and tissue growth in order to regenerate living tissues for therapeutic purposes [1]. TE is a multidisciplinary field that involves materials science and engineering, which provide the adequate knowledge for the design and manufacture of the supports and the nutrients transport mechanisms, and biology principles that procure the necessary basis to understand biological systems [2].

The description of the TE principle is briefly presented in Figure 1.1. The in vitro tissues are obtained from the extraction, isolation and expansion of the patient's cells that are cultured on a cellular support (scaffold). The cell seeded scaffold is transferred to a bioreactor where the cells proliferate until they differentiate in the target tissue. They grow in vitro and obtain the functionality of the organ to be reproduced. Finally, the tissue constructed could be transplanted in the patient.

A recent application of TE has been developed. In this application, the regenerated tissue could be used as model to study biological mechanisms, therapeutics, etc., as alternative to animals' models. It could be possible to develop in vitro neuronal or cellular models in order to investigate different disease mechanisms or as screening of new drugs [3]. This opens the door to the development of personal/tailor-made treatments created for the patient.

Successful in vitro tissue engineering strategies require an adequate source of cells, optimization of scaffolds structure and design of bioreactors.

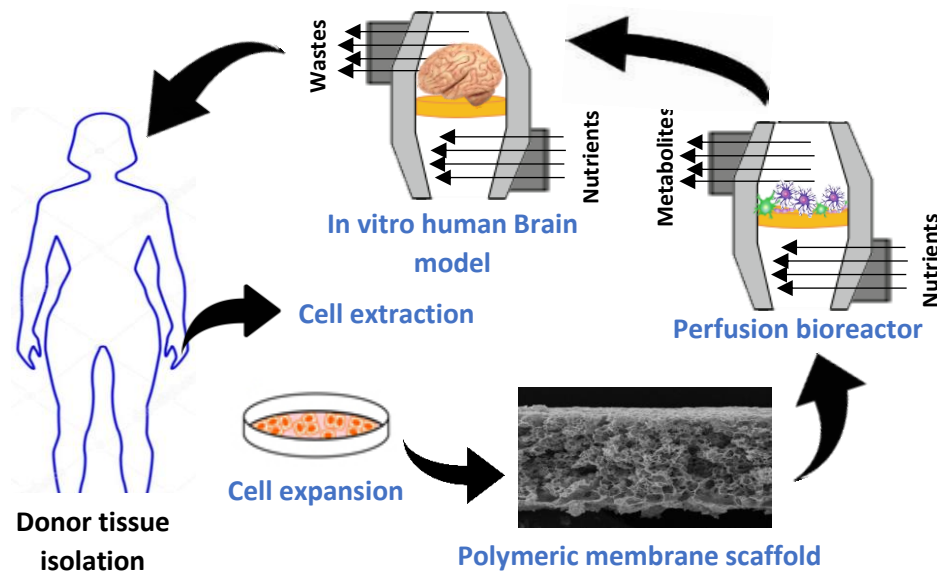


Figure 1. 1. Schematic diagram of tissue engineering principle using flat sheet polymeric membranes as scaffolds and tangential diffusion perfusion bioreactor

1.2. TISSUE ENGINEERING BIOREACTORS

Bioreactors (BRs) are an important part of TE aiding the construction of three-dimensional functional tissues. The main function of a bioreactor (BR) is to provide an adequate biomechanical and biochemical environment and favor the supply of nutrient and oxygen to the cells and to remove metabolic products.

The BR requires both the biological and engineering fields to be addressed, as well as the problems of reliability, reproducibility and security in the system. The BR system presents advantages in terms of low contamination risk, ease of handling and scalability [4]. It is crucial to have a good mass transfer and mechanical stimulation for culture conditions. Besides, shear stress to the cells should be controlled.

Table 1.1 shows a comparison between different TE BR. BRs can be generally divided into static and dynamic. Sub-classification of BRs depends on geometry and/or functions customized for the particular tissue growth [5]. The BRs offer three types of flow conditions (static, laminar and turbulent) that cause different speeds of nutrient supply and shear stresses on the cell culture.

Cell maintenance and proliferation is usually performed in static culture systems (See Table 1.1) with a monolayer of adherent cells. These systems enable sterile handling

procedures and are easy to use, disposable and low-cost. However, they require individual handling as for example in medium exchange. Moreover, cell seeding and increase in cell numbers above 2D cell monolayers is limited [4]. Static culture presents nutrient limitations since both external and internal mass transfer are undertaken by diffusion mechanism appearing concentration gradients with local depletion of nutrients and accumulation of waste material [6]. In consequence of that, dynamic BRs appear.

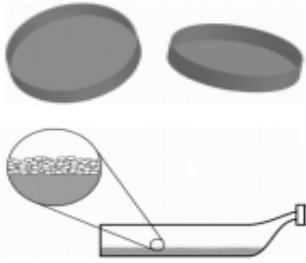
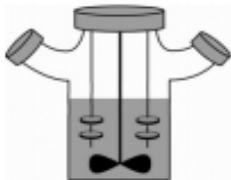
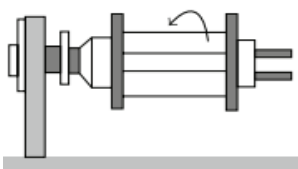
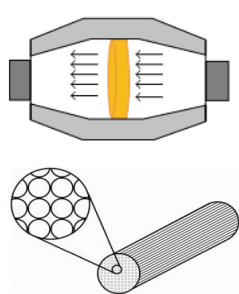
Several researches done exhibit the development of BR to grow 3D tissues, which designs introduce stirring (Stirred tank, Table 1.1) or rotation (Rotating wall, Table 1.1) in order to reduce the convective resistances of the nutrients in the proximities of the cell construct. However, the diffusional resistance still persists due to the difficulty of the tissue constructs for developing neovascularization [7]. The solution found is promoting flow perfusion through the scaffolding (Perfusion BRs, Table 1.1).

1.2.1. Perfusion Bioreactor

In perfusion BRs, cells grow in porous scaffolds. Culture medium is perfused directly around or through cells forcing the convective transport of nutrients [6]. Perfusion BRs offer better control of mass transfer than other conventional systems. They reduce the internal and mostly external diffusive limitations for nutrient transport. Furthermore, perfusion BRs enable the application of mechanical stimuli on cultured cells improving tissue growth being able to sustain cell culture environments [8].

One of the major problems of perfusion BRs is that they choose preferential paths through the system and cause shear stress on cells [6]. The preferential route, occurs in scaffolds with a high pore size distribution and in tissues that do not develop uniformly, leaving some regions poorly nourished, while others perfuse strongly. Thus, it is important to establish an adequate pressure in the system for the correct proliferation and growth of cells without produced shear stress. To overcome this, hollow fiber membrane bioreactors (HFMBs) prompted out, operating under perfusion conditions, try to mimic physiological vascular networks using 3D scaffolds giving more benefits because of tangential perfusion.

Table 1. 1. Different tissue engineering bioreactors [5], [6]

Bioreactor type	Description and considerations
Static culture 	<ul style="list-style-type: none"> - Batch culture: no flux of nutrients - High nutrients diffusion limitation - Very low cell proliferation - Homogeneous structure of cell constructs
Dynamic bioreactors	
Spinner flask/ Stirred tank 	<ul style="list-style-type: none"> - Mechanical and magnetic agitation - Poor mass transfer - Easy to scale up - High shear stress - Used in dynamic seeding
Rotating Wall BR 	<ul style="list-style-type: none"> - Constant speed of rotation - Suitable for growing large tissue mass - Complex system, not easily scalable - Low shear stress - Used in laminar flow conditions
Perfusion BRs 	<ul style="list-style-type: none"> - Cells seeding and attachment within the scaffold - Stable microenvironment, good distribution of nutrients and uniform cell distribution - Moderate-low shear stress - Used in to develop relevant human tissues

In perfusion BRs, scaffolds play a crucial role in the reconstruction of diseased tissues due to their porous, biocompatible and non-toxic characteristics. The scaffold material could be natural or synthetic. However, a biodegradable polymeric material is preferred as it avoids potential immune response from naturally derived materials of animal

origin. They also must have an interconnected network for easy access of nutrients and removal of metabolic wastes into and from cells [9]. Particularly, in HFMBs, polymer membranes are used as scaffolding materials due to their high porosity and nutrients transport properties. It is known that the behavior of cells under in vitro culture conditions is influenced by the structure of the scaffolds, which depends on the manufacturing method employed. Phase inversion is arguably one of the most common and versatile technique used to prepare all sorts of morphologies of polymer membrane scaffolds [10].

Membrane scaffolds made of poly (ϵ -caprolactone) (PCL) polymer with nanoparticles of reduced graphene oxide (rGO) by phase inversion present a lot of advantages when neural in vitro regeneration is pursued. The rGO induces electrical activity in neural cells and furthermore, these PCL/rGO membranes present unique outstandingly porous morphology guaranteeing high permeance of nutrients and favoring cellular adhesion and proliferation. Studies of in vitro hydrolytic degradation carried out on those PCL/rGO membranes reflect that the gradual degradation of the PCL/rGO membranes could facilitate cell infiltration, interconnectivity and tissue formation [11].

Finally, fouling phenomena in biocompatible scaffolds is one of the critical factors. Fouling governs the effectiveness of many microfiltration processes caused by the deposition of protein aggregates onto the membrane surface forming a cake [12]. Besides, protein adsorption favors cell adhesion to the scaffolds.

1.3. OVERVIEW OF MATHEMATICAL MODELS DESCRIBING MASS TRANSPORT OF NUTRIENTS IN PERFUSION BIOREACTORS FOR TE

It is essential to use mathematical equations and modeling techniques to simulate the optimal operating conditions and to procure more efficient tools for perfusion BRs design.

Diverse studies have concluded that oxygen supply in 3D tissue constructs in vitro is a critical parameter being the only nutrient that is provided continuously. It influences in self-renewal, maintenance and cell differentiation [13]. Usually, the major restriction comes from the cell layer since scaffolds do not offer much resistance to its transport.

Only in cell layers with a maximum thickness of 100-200 μm , O_2 can be supplied correctly by diffusion [14].

A mathematical model for transferring oxygen in a hollow fiber bioartificial liver has been developed [15]. The work presented the diffusion transport limitations for this critical nutrient in 3D tissue regeneration describing the cellular oxygen consumption on Michaelis-Menten kinetics.

In terms of nutrient transport and consumption, oxygen is the most widely modelled solute but glucose and proteins have also been considered. Some mathematical models represented the nutrient transport (glucose and O_2) and cell growth of chondrocytes studying the dynamic and mass transport by diffusion and convection in a perfusion BR [16]. For that, the model used computer fluid dynamics (CFD) software as computational tool to represent the fluid flow through the 3D scaffolds and to provide quantitative information of the velocity and shear stress distribution within it.

By contrast, the transport of lactate, a waste product of cell metabolism toxic to cells in high concentrations, has only been modelled recently in HFMBs in order to predict the operating conditions that maximize the chondrocytes and hepatocytes cells layer growth for different cell types [17]. The cells seeded on the outer surface of a single fiber in the HFMB. Flow equations are coupled to reaction–advection–diffusion equations for oxygen and lactate transport through the perfusion BR. However, further research is required to establish appropriate operating conditions for expanding different cell types (for example, neuronal cells) in perfusion BRs.

There is a lack of models that take into account the phenomenon of fouling by protein deposition in the scaffolds used in perfusion BRs. It is known that during the first hours of the experiment, this phenomenon is very important for controlling the adhesion and cell proliferation [18]. If it is not modeled, it prevents a correct description of the phenomena that occur in the system. In addition, no works reporting mathematical models describing the nutrients and metabolites transport and proliferative behavior of neuronal regeneration in in vitro membrane perfusion BRs have been found. Therefore, a realistic mathematical model that takes into account the protein fouling phenomena on the membrane scaffold and that can be applied to a tangential flow perfusion BR in

flat configuration for the accurate description of neuronal cell proliferation is needed in the present proposal.

1.4. OBJECTIVES

In the Environmental and Bioprocess Technologies (TAB) research group, which is part of the Department of Chemical and Biomolecular Engineering of the UC, there is a line of research dedicated to the development of new polymeric membranes as scaffolds and the design of new perfusion BRs for TE. The investigation centers on the manufacture of membranes that act as cellular support for the regeneration of neural tissue, induce neural differentiation and facilitates high nutrients supply and metabolites removal for in vitro perfusion BRs.

The present project focuses on the design, assembly and tune up of a membrane perfusion BR to address regeneration of neuronal tissue under dynamic culture. Within the system, an oximeter will be calibrated and tuned for an exhaustive control of O₂.

The biocompatible and biodegradable microfiltration membranes of PCL functionalized with rGO that enhances the differentiation of stem cells in neuronal cells, will be synthesized using the phase inversion technique. The diffusive and convective transport properties of nutrients of these membranes will be characterized prior to dynamic cell culture tests. Fouling phenomena of the membrane due to the presence of BSA protein on the culture medium will also be studied using model BSA solutions.

To simulate the nutrients consumption and metabolites production during in vitro cell proliferation stages, a mathematical model of the system will be made in Aspen Custom Modeler (ACM). In this way, it will be seen the theoretical influence of transport and consumption of the most important nutrients such as glucose and oxygen and the production of lactate as metabolite on the metabolic activity of the cells. The model could be used to optimize the operation variables as well as to help in the estimation of cells consumption parameters for future experimental testing.

All work developed will serve as a prelude to demonstrate the potentiality of the perfusion system to be used in the proliferation of neuronal stem cells to regenerate in vitro tissue that has synaptic brain functionality.

2. DEVELOPMENT

2.1. EXPERIMENTAL SETUP

The experimental setup is depicted in Figure 2.1. The purpose of the complete system is to achieve the differentiation of stem cells in neuronal cells in in vitro culture systems. It was formed for several elements that are explained below.

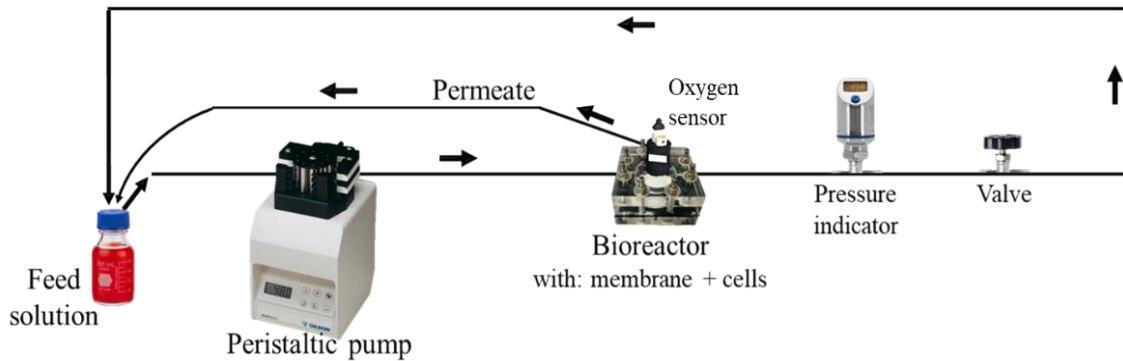


Figure 2. 1. Experimental setup

- **Perfusion cell**. The perfusion cell was the principal part of the perfusion BR system. It consisted of 3 main pieces that could be seen in Figure 2.2. The bottom piece, which was the vascular chamber, simulated the vascular system in the human body. The intermediate piece was the cellular chamber in which cells could be cultured and grow. Finally, the cover of the BR was a top piece fixed with screws at 0.8 Nm of pressure applied with a torque wrench. All parts of the perfusion cell BR were made of an experimental resin. A physical barrier existed between the vascular and cellular chamber, it was the polymeric PCL/rGO scaffold manufactured during this work. The microporous membrane acted as a support for the adhesion and proliferation of the cells.

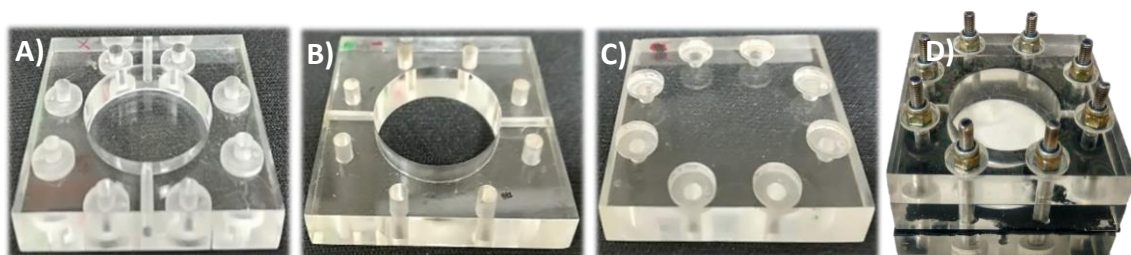


Figure 2. 2. A) Vascular chamber, B) Cellular chamber, C) Top piece and D) Perfusion cell assembled

Perfusion cell BR only could be cleaned with ultrapure water besides autoclaving. It cannot be used alcohols or organics dissolvent to sterilize the BR because causes damages in the BR material and in cells.

- **Membrane.** To obtain the PCL/rGO membrane, a method developed in the TAB group was reproduced. The reduced graphene oxide (rGO) was synthesized using a hydrothermal method through commercial graphene oxide (GO) (Avanzare, Innovacion Tecnologías S.L.).

In brief, the GO was dispersed in UP water (UP W, MilliQ, Millipore). ($C_{GO} = 0.5 \text{ mg/mL}$) by sonication (20'). The mixture was kept inside a Teflon lined autoclave and heated at 200°C during 3 h. At last, the obtained rGO was dried at 50°C for 1 day.

Because of phase inversion is a fast and cheap method that can be easily used and allows the fabrication of reproducible membranes of different polymeric materials, it was employed for doing the PCL/rGO flat membranes.

The polymeric solution was composed of 15% w/w of poly-ε-caprolactone (PCL, Sigma-Aldrich, MW: 80000 Da), 0.1% w/w of reduced graphene oxide and N-methyl-2-pyrrolidone (NMP, 99%, Extra Pure, Across Organic). The procedure followed was:

- 1) Dispersion of rGO in NMP using ultrasonication during 30'.
- 2) Addition of PCL in the rGO/NMP dispersion and stirred using a roller agitator (Roller Shaker 6 Basic, IKA) for 48h at 37°C to reach homogenization. Later, the polymeric solution was left rest 24h for degassing at room temperature.
- 3) The solution was casted on a glass plate using a doctor blade casting knife (3580/2, Elcometer) through a 200 μm slit with the same force applied to have a uniform membrane.
- 4) Subsequent, the casted solution was immersed in a coagulation bath composed of isopropanol (IPA, 99.9%, Oppac), aiming at the polymer precipitation. IPA was used as coagulant bath to obtain higher roughness and porosity, comparing to other non-solvents [19]. In consequence, the membranes present high and interconnected poros, resulting in high permeances favoring higher cell growth.
- 5) Once the polymer film was precipitated, membranes were transferred to a second coagulation bath with the same composition for 1 day to ensure the complete solvent exchange.

- 6) Later, it was really important remove completely traces of the solvent and non-solvent by immersing the membranes into a bath of UP during 48 h changing it 3 times a day for not causing several damages to the in vitro system if there was.
- 7) Finally, membranes were dried at room temperature.

The sterilization for the membrane would consist on immerse it on 70% ethanol solution as it melts at temperatures above 60 °C [8].

- **Oximeter**. Oximeter was a contactless oxygen sensing system (BlueBlink, EBERS Medical Technology S.L) for continuously monitoring of the oxygen nutrient in cell culture chamber. It was made of two basic parts: an optical reader and a sensing spot sterile ready to use. It could measure in continuous and discrete mode and in different units and ranges.

- **Pressure Indicator**. It was a precision pressure transmitter with switching contacts and display (JUMO DELOS SI) that was installed in the system. The range measurement of the device went from 0 to 0.4 bar of pressure suitable for the application performed. It provided accurate measurements.

- **Peristaltic Pump**: Peristaltic Pump - MINIPULS 3, GILSON® was used to feed the system with tubes made of silicone elastomer with an internal diameter of 1 mm and external diameter of 4mm. The tubes had excellent biocompatibility used in biological applications and it could be autoclaved or uv-irradiated for sterilization. The pump had adjustable head speeds from 0-48 rpm. The pump was calibrated (see *Appendix A: Peristaltic Pump Calibration*).

- **Valve**: Stainless steel needle valve of HOKE was used to pressurize the system.

The system was introduced in an incubator that worked at constant temperature (37 °C). It was used to simulate the desired conditions during dynamic cell culture and was tested with different feeding solutions.

The sterilization protocol was proposed and carried out, simulating that there were cells in the system. First, all constituents were autoclaved. To do so, a program with an autoclave was executed at 120 °C during 30 min. Second, to introduce the components in the incubator all components less the BRs were sterilized using ethanol solution.

2.2. MEMBRANE CHARACTERIZACION

2.2.1. Membrane thickness

The thickness of the membrane (δ) was measured by an electronic micrometer (Standard Model, Series 293, Mitutoyo).

2.2.2. Water flux membrane characterization

A homemade cross-flow filtration setup (see *Appendix B: Cross-flow filtration setup*) was used for the characterization of water flux of the PCL/rGO membranes at 37°C using a 90 mL min⁻¹ flowrate of feed liquid. The water permeate flux was measured at fixed pressure values during up-down pressure cycles within 0.04 to 0.20 bars for each membrane specimen.

2.2.3. Glucose diffusivity in PCL/rGO scaffold

The diffusivity of glucose across the PCL/rGO scaffold was determined using a diffusion cell (Figure 2.3). The PCL/rGO membranes were immersed in a 70% ethanol solution for one day before the diffusion tests. The diffusion cell consisted of two equal cylindrical compartments ($\varnothing = 6.5$ cm, $h = 8.2$ cm), that were connected by the PCL/rGO membrane ($A = 15.9$ cm²).

The diffusion cell worked at steady state conditions and at room temperature (25 °C) to avoid water evaporation produced at 37°C in the water compartment. Both compartments employed an agitation of 2 RPM to facilitate the diffusion.

Initially, one compartment was filled with 280 mL of 5 g/L of D-glucose (Sigma Aldrich, $\geq 95\%$, powder) in UP and the other compartment was filled with 280 mL of UP. Samples of 0.4 mL were taken simultaneously from both compartments using a micropipette to quantify the diffusivity. The measurements were taken at daily intervals. The diffusion studies were conducted until equilibrium was achieved.

The concentration of glucose was analyzed in both compartments using a UV-vis spectrophotometer (UV-1800 Shimadzu) at a wavelength of 500 nm. The procedure was described in *Appendix C: Glucose and lactate quantification protocols*. Experiments were repeated to check the reproducibility of the results.

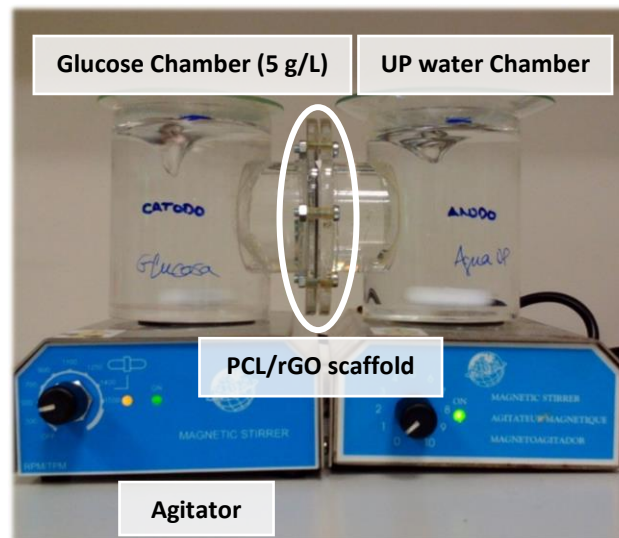


Figure 2. 3. Diffusion cell with glucose and ultrapure water compartments, connecting by the membrane

2.3. BIOREACTOR FLUX EXPERIMENTS

2.3.1. Oxygen sensing system calibration

An oxygen sensing system (BlueBlink O₂ sensing system, Ebers Medical Technology S.L.) was tuned up. The instrument consists of an optical reader that measures the O₂, a sensing spot which is useful to determine the concentration of O₂ based on the fluorescence quenching physical phenomenon and the controlling software.

The sensing spot contains a fluorescent substance that, with a short delay after being excited by the optical reader, emits light with a different wavelength. The intensity and time delay of the emitted light depend on the partial pressure of oxygen. The reader optically filters and measures such emitted light, using that measurement to calculate the O₂ concentration. This device was biocompatible. The tasks developed during the installation and set-up of this device were classified into:

1. **Installation** of the BlueBlink Oxygen Sensing System program.
2. **Sticking spots to vessels and BR.** The sensing spots were in contact with the liquid medium to measure the oxygen content. They were disposable, self-adhesive and attached to the inner surface of a transparent wall. Each spot is composed of five layers (Figure 2.4).

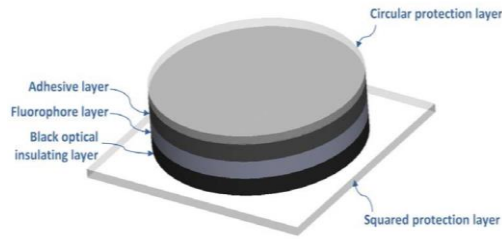


Figure 2. 4. Sensing spot layers

- 3. Calibration.** The instrument should be calibrated in the same environmental conditions as the experiment will be carried out. Thus, the instrument was calibrated simulating the incubator conditions: 37°C of temperature, 1013 hPa of pressure and 95% of humidity. The calibration was divided in two points of calibration:

- ❖ Calibration at 100% air-saturated conditions. Air was supplied into a beaker using distilled water with agitation during 15 min at atmospheric pressure. After that, the liquid stabilized during 5 min in the beaker and then, 1 min in the beaker with the spot to calibrate the sensor at 100% air-saturated conditions.
- ❖ Calibration at 0% air-saturated conditions. Na₂SO₃ was added in the water container (2.5 g/L) in order to eliminate all the oxygen, according to the following reaction (R. 1):



After the agitation of the mixture during 1 min, it was filtered and passed to the beaker with the spot to calibrate the sensor at 0% air-saturated conditions.

- 4. Experiments.** Once calibrated, many experiments have been carried out (Table 2.1). The measurement was done in continuous and discrete form. Figure 2.5 presents the oxygen sensor a) with the spot in the alimentation tank and b) with the perfusion cell.

Table 2. 1. Experiments done with the oximeter at 37 °C

Liquid Medium	Work conditions
Deionized water (W, Elix)	With and without recirculation (50 rpm)
Tap water	With and without recirculation (50 rpm)
Culture medium: DMEM	With recirculation (9 rpm)

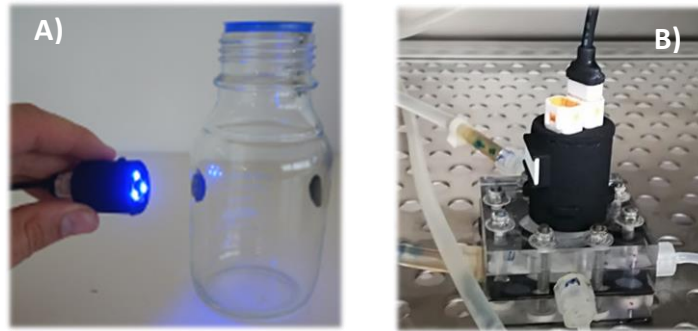


Figure 2. 5. A) Oxygen sensor and alimentation tank with spot, b) oxygen device + perfusion cell

To analyze the performance of the oximeter on a real cell perfusion BR system a preliminary dynamic cell culture was carried out as is explained in *Appendix D: Dynamic cell culture*. The objective of this experiment was to monitor the oxygen concentration in the BR cell chamber with the oximeter during dynamic cell culture and check if the oxygen was a limiting nutrient during the timeframe in which the experiments would be conducted in future BR tests.

In view of the results after 7 days and the difficulties found carrying out this dynamic experiment with reproducibility and tightness, it was confirmed the need of accomplish a more thorough analysis of the tuning, optimization, assembly, etc. of the system equipment and operational variables, proceeding to perform the following analyzes in the absence of cells.

2.3.2. Water experiments

Preliminary experiments with water were performed in order to solve some detected problems: reducing the length of silicone tubes in order to minimize the dead volume (down to 15 mL), avoiding leakages, set a controllable pressure in the system, avoiding the formation of bubbles, etc.

The filling up and removal of air bubbles is one of the critical steps when cells have to be introduced in the system. Therefore, a careful protocol has been developed: First, UP water was pumped into the BR perfusion system with the peristaltic pump (1 mL min^{-1} of feed flowrate). Next, for filling the perfusion cell, the feed solution entered by the impulse of the peristaltic pump through the vascular chamber. At that moment, the cellular chamber had been opened to the atmosphere until the vascular chamber was

filled and recirculation began to the feed tank. Then, the cellular chamber aperture was closed to pressurize the flux from the vascular chamber to the cellular chamber. Manipulating with valve, the pressure increased in the system and permeate appeared loading the cellular chamber. Changes in transmembrane pressure were observed in the behavior of the scaffold that bulged or went down. It was really important to control the transmembrane pressure that is exerted in the perfusion cell to control the constant flow nutrients from vascular chamber to cellular chamber.

The transmembrane pressure, permeate flux and oxygen concentration was measured making changes in connections, valve and others to control and calibrate the system.

2.3.3. BSA+Glucose model solution filtration tests

After water assays, perfusion tests of a nutrient model solution has been carried out for 3 days. Tests were replicated 6 times at different inlet flowrates (4.5 rpm and 48 rpm). The system was tested with a model solution of Bovine Albumin Serum (BSA, 0.4 g/L) and glucose (1 g/L) dissolved in a phosphate buffered saline (PBS) at pH 7.4 under simulated cell culture conditions.

BSA proteins are the most abundant soluble proteins of the circulatory system possessing outstanding functions at a biological and pharmacokinetic level. It is not a direct nutrient of cells such as oxygen or glucose. However it is not possible to develop a culture system in the absence of BSA because cell growth does not occur [20].

PBS is a buffer solution commonly used in biological research because the composition and the osmolarity match those of the human body. It helps to maintain a constant pH at 7.4. The PBS solution was prepared as follows:

First, the mixture of reagents showed in Table 2.2 in 800 mL of deionized water was made resulting in a water-based salt solution. Next, the mixture was adjusted at 7.4 pH with HCl and finally, H₂O was added until 1L of solution.

The transmembrane pressure, permeate flow and transmittance of the BSA model and glucose through the membrane, necessary to guarantee the feeding of the cells supported on the membrane, were monitored.

Table 2. 2. PBS composition

Components	Mass (g)
Sodium Chloride (NaCl)	8
Potassium Chloride (KCl)	0.2
Disodium hydrogen phosphate (Na ₂ HPO ₄)	1.44
Potassium dihydrogen phosphate (KH ₂ PO ₄)	0.24

Samples were taken 2-3 times per day for both cellular chamber (permeate) and feed tank solution (recirculation + permeate). With the samples, the total permeate volumetric flowrate was measured.

The BSA concentration in the feed and permeate streams was measured using UV spectrometry (UV-1800 Shimadzu) at a fixed wavelength of 280 nm. PBS solution was used as blank. The concentration of glucose was also analyzed in both streams by UV-vis spectrometry at a wavelength of 500 nm following the procedure explained in *Appendix C: Glucose and lactate quantification protocols*.

The procedure to see the evolution of lactate concentration as the main metabolites produced during cell culture was also tuned for future dynamic experiments with cells. The procedure was likewise described in *Appendix C: Glucose and lactate quantification protocols*.

2.4. MODELLING WITH ASPEN CUSTOM MODELER

In order to gain better understanding on how physical factors modulate tissue development, it is necessary to integrate BR studies with quantitative analyses and computational modeling to predict changes in mass transfer of nutrients and additionally evaluating the physical forces experienced by cells [6]. A mathematical model in Aspen Custom Modeler was developed aimed at describing the supply and transport of nutrients (glucose and oxygen) to the neural cells selected in the present work (U87 glioblastoma cells), the production and removal of toxic metabolites (lactate) from cells and the fouling mechanism due to the BSA protein through the PCL/rGO scaffold in the perfusion BR. The different assumptions considered in the perfusion cell BR are as follows:

Membrane fouling:

A highly porous scaffold is necessary to ensure the sufficient nutrient transport and promote the cell attachment and proliferation. However, many studies reported the fouling phenomena in polymer porous membranes due to protein solutions. Fouling results in a decline of permeate flux because increases the total resistance by decreasing the available pore area or creating an additional layer that exerts resistance to the flux, preventing the correct perfusion of the nutrients in the system. Adherence and initial stages of the proliferation occur usually simultaneously to the appearance of the fouling phenomena. For that, different fouling mechanisms were analyzed fitting the experimental data and selecting the appropriate fouling mechanism presented in the PCL/rGO membranes during the experiments, as transient transport behavior of membranes might affect these initial stages of cell growth.

The basic fouling mechanisms are the following: 1) the protein adsorption to the membrane, 2) the deposition of protein within the pores or at the pore entrance and 3) cake layer formation on the membrane [21]. The external fouling occurred by the deposition of protein aggregates due to the formation of disulfite bonds between BSA molecules creating a deposited cake on the membrane surface and the internal fouling of the membrane was produced by the interactions between proteins and the pore surface when the pores are sufficiently large to allow protein aggregates intrusion [12]. Table 2.3 shows the linearized forms of the classical filtration models, which were used for data analysis and identification of fouling mechanisms.

The flux through the membranes accounting with the incorporation of a fouling mechanism expressed in terms of resistances in series can be derived from Darcy's Law (Eq. 1). The effect of fouling generates an extra resistance in addition to the membrane resistance.

$$J = \frac{\Delta P}{\mu \cdot (R_m + R_f)} \quad (1)$$

For instance, considering the fouling mechanism of cake formation, assuming that the formation of cake is constant and equal to the convective solute transport at steady

state, because is the phenomena prevailing in this system, the fouling resistance can be calculated from:

$$R_f = \alpha_f \cdot C_b \cdot \left(\frac{V}{A_m} - J_{ss} \cdot t \right) \quad (2)$$

Being α_f the intrinsic resistance of the cake, V the permeate volume and J_{ss} the steady state permeate flux.

Table 2. 3. Empirical dead-end filtration equations [21]

Law	Description	Equation
Intermediate blocking	Occlusion of pores by particles with particle superimposition	$\frac{1}{J} = at + b$
Complete blocking	Occlusion of pores by particles with no particle superimposition	$-\ln\left(\frac{J}{J_0}\right) = at + b$
Cake filtration	Deposit of particles larger that the membrane pore size onto the membrane surface.	$\frac{t}{V_{ac}} = aV_{ac} + b$

Where V_{ac} is the cumulative volume of permeate at time t , J is the permeate flux, J_0 is the initial permeate flux, and a and b are empirical model parameters.

However, more than one fouling mechanism could occur. In this way, a combined mathematical model was developed [22] for initial fouling due to pore blockage (first term Eq. 3) and subsequent fouling due to the growth of a protein cake or deposit over these blocked regions (second term Eq. 3). The model can be expressed as:

$$J = J_0 \cdot \left\{ \exp\left(-\frac{\alpha \cdot \Delta P \cdot C_b}{\mu \cdot R_m} \cdot t\right) + \frac{R_m}{R_m + R_f} \cdot \left(1 - \exp\left(-\frac{\alpha \cdot \Delta P \cdot C_b}{\mu \cdot R_m} \cdot t\right)\right) \right\} \quad (3)$$

Where J_0 is the volumetric flux through the clean membrane, ΔP is the transmembrane pressure, C_b is the bulk protein concentration, R_m is the resistance of the clean membrane, and α is the pore blockage parameter. With the resistance of the protein deposit, R_f , as:

$$R_f = (R_m + R_{f0}) \cdot \sqrt{1 + \frac{2 \cdot \beta \cdot \Delta P \cdot C_b}{\mu \cdot (R_m + R_{f0})^2} \cdot t} - R_m \quad (4)$$

Where R_{f0} is the resistance of a single protein aggregate and β is the rate of increase of the protein layer resistance with time. These parameters were obtained from experimental data as it was seen in *Appendix E: Mathematical model development*.

Diffusion plus convection on membrane layer and cell layer:

During in vitro culture, mass transport through the membrane and the cell layer occurs as the result of convection and diffusion process [23]. Both mass process in both layer were analyzed.

Membrane exerts a resistance to the mass transport because of being a physical barrier. It is important to evaluate the diffusion process across the scaffold to check if the mass transport is favored or not. In the case of cells, if the thickness of the layer is high, there will be nutrient shortage, limiting cell proliferation. Moreover, cells could consume nutrients faster than the rate of nutrients supplied by diffusion [23].

Due to the forced convection or perfusion exerted to the system, it was considered concentration polarization negligible.

Cell growth kinetics, nutrients consumption and metabolites production:

It was assumed that the main nutrient for glia cells was glucose as carbon substrate and oxygen for cellular respiration, and the main metabolite product of the biological cell process was lactate. The rest of nutrients are considered to be present in excess in the culture medium. It was supposed that cells were attached to the surface membrane.

Michaelis-Menten kinetics for oxygen cell consume was used [24] and besides, several articles in literature [25] suggest a mathematical model for oxygen considering the changes in the spatial position (x , y and z), here the concentration of oxygen is assumed to be constant across the length and width of the scaffold to simplify the model. Model of Monod growth kinetics for biomass were adapted for the system [26]. No values of neuronal cells were found in literature for Monod coefficients used in glucose and lactate balances, so other values for cellular systems reported were used [27, 28]. For oxygen parameters, values of neuronal tissues were used.

Models and simulations:

The system consisted in a feeding tank (perfect mixing) that fed continuously the perfusion cell. Therefore, a set of connection equations in both elements were defined. These equations included the total and component mass balances for the nutrients and products, counting the cellular growth and fouling mechanism.

All was implemented in ACM and a sensitivity analysis of the variable volume and biological parameters predicting the nutrients consumption and metabolites production was done. The unknown parameters of Eq.3 and 4 for combined fouling mechanism were obtained by parametric estimation with ACM.

The complete mathematical model with all the equations and meaning terms could be seen in *Appendix E: Mathematical model development*. A summary of the different parameters used in the model and the operational conditions could be seen in Table 2.4 and 2.5.

Table 2. 4. Parameter values used in simulations

MODEL PARAMETERS			
Parameter	Value	Unit	Reference
μ_{PBS}	$1.94 \cdot 10^{-12}$	bar h	[29]
R_m	$2.66 \cdot 10^{11}$	m^{-1}	*
K_m	1.022	$m^3 m^{-2} h^{-1} bar^{-1}$	*
αf	$1.67 \cdot 10^{14}$	$m kg^{-1}$	*
Cb	0.4	$kg m^{-3}$	*
J_{ss}	$2.20 \cdot 10^{-6}$	$m^3 h$	*
Vol_v	$2.77 \cdot 10^{-6}$	m^3	*
Vol_{cell}	$5.46 \cdot 10^{-6}$	m^3	*
A_m	$6.16 \cdot 10^{-4}$	m^2	*
$D_{O_2, cell}$	$5.76 \cdot 10^{-6}$	$m^2 h^{-1}$	[25]
$C_{O_2, cell}$	$6.74 \cdot 10^{-3}$	$kg O_2 m^{-3}$	[25]
q_{O_2}	$8.87 \cdot 10^{-14}$	$kg O_2 cell^{-1} h^{-1}$	[26]
m	0.57	$kg glucose kg cell^{-1} h^{-1}$	[28]
$mass_{cell}$	$27 \cdot 10^{-15}$	kg	[30]
x_{cell}	$10 \cdot 10^{-9}$	m	[31]
Y_{XS}	0.013	$kg cell kg glucose^{-1}$	[28]
Y_{PS}	0.73	$kg lactate kg glucose^{-1}$	[28]

* Experimentally determined model parameter

Table 2. 5. Operating conditions

OPERATING CONDITIONS		
Variable	Value	Unit
ΔP	0.023	bar
V	$100 \cdot 10^{-6}$	m^3
Fi	$6 \cdot 10^{-5}$ and $5.1 \cdot 10^{-4}$	$m^3 h^{-1}$
T	37	$^{\circ}C$
V_{sample}	$8.33 \cdot 10^{-8}$	$m^3 h^{-1}$
t	120	h

Due to the results obtained, which are going to be explained in the next point, the following simplifications can be assumed in the present work:

- Changes in volume occurred as a result of sampling.
- The thickness of the glioblastoma cells layer proliferated was supposed to be a monolayer and the time of culture (5 days) was not sufficient to achieve the confluence. So, the resistance due to the diffusivity across cell layer could be neglected. Besides, the convective flux is supposed to be much higher than the diffusion one. For that reason the term of diffusion mass transport was neglected.
- For oxygen, only changes in the cellular chamber were evaluated, considering that the rest of the system was saturated in O_2 . Because of the smaller diameter of the oxygen, all passed through the scaffold without limitations.
- To study the fluid medium and its movement, the PBS was taken as reference.

3. RESULTS AND DISCUSSION

3.1. MEMBRANE CHARACTERIZATION

In the present work, the thickness and the transport properties of the PCL/rGO were characterized to verify the reproducibility of the membranes already made.

The thickness (δ) of the flat membranes obtained was $100 \pm 6 \mu\text{m}$, corresponding with the thickness of the previous work [8]. In Figure 3.1, the clean water fluxes ($\text{L m}^{-2} \text{h}^{-1}$) at different transmembrane pressures are presented. The hydraulic permeance was $1022 \pm 169 \text{ L m}^{-2} \text{h}^{-1} \text{bar}^{-1}$.

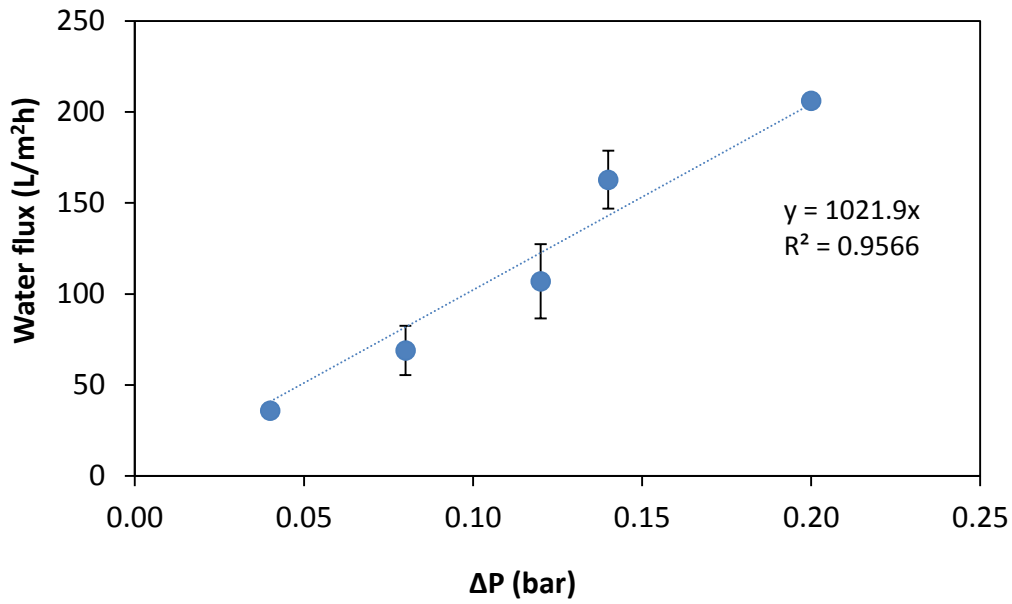


Figure 3. 1. Clean water flux for PCL/rGO at different transmembrane pressures

Compared with previous characterizations [8], these PCL/rGO membranes presented significantly lower water fluxes and hydraulic permeances attributed to experimental error on the batch prepared. However, the permeabilities attained were still comparable to other membranes reported in the literature for cell TE in BRs (Table 3.1). For instance, the PCL hollow fibre membranes in ethanol coagulation bath to be used as small blood vessel scaffolds presented a hydraulic permeances of $800 \text{ L m}^{-2} \text{bar}^{-1} \text{h}^{-1}$ [32]. Similarly, the permeance of poly(l-lactic acid) hollow fiber membranes for artificial vasculature in TE scaffolds was $2094 \text{ L m}^{-2} \text{bar}^{-1} \text{h}^{-1}$ [33]. Another scaffolds made of PEEK-WC used in perfusion BRs with human lymphocytes exhibited similar permeances than the present work [34].

3. RESULTS AND DISCUSSION

Table 3. 1. Comparison of the hydraulic permeances of the PCL and PCL-graphene membranes with other polymer membranes reported in the literature

Membrane material	Hydraulic permeance ($\text{L m}^{-2} \text{ bar}^{-1} \text{ h}^{-1}$)	Reference
PCL/rGO	1022±169	Present work
PCL	800	Diban et al [32]
PLLA	2094	Bettahalli et al [33]
PEEK-WC	758	De Bartolo et al [34]

3.1.1. Glucose diffusion coefficient

Glucose is the main nutrient in neuronal cells, therefore it is important to determine the effective glucose diffusion coefficient in the porous scaffold to understand the importance of nutrient diffusion through the membrane scaffold used in the present application.

The evolution of glucose concentrations in glucose compartment and water compartment with time under room temperature are depicted in Figure 3.2. Although experiments at 37°C were tried, the evaporation of the water in the compartment of UP water occurred. Therefore, to avoid experimental error, tests were done only at room temperature.

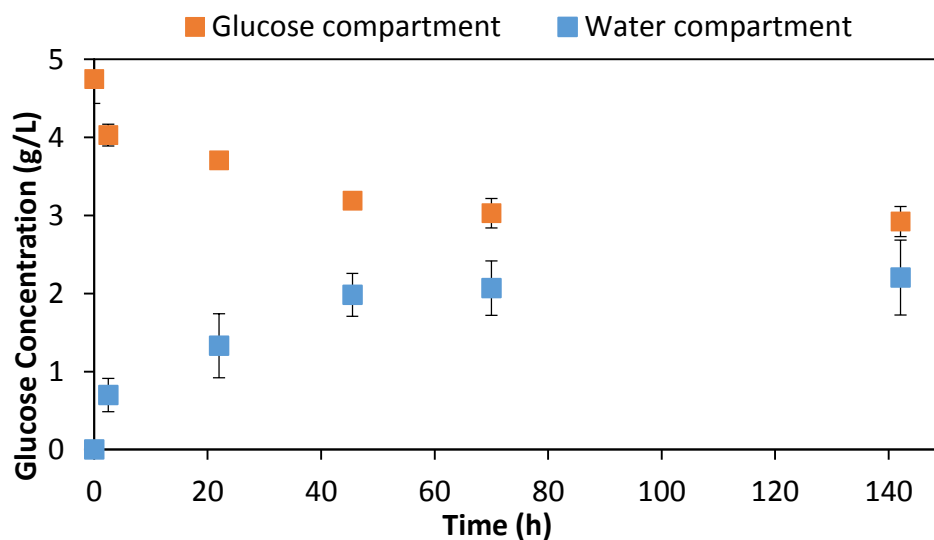


Figure 3. 2. Evolution of glucose concentration with time of diffusion cell experiments in PCL/rGO scaffolds at room temperature

As it could be seen there was a progressive decrease in the glucose concentration in the glucose compartment, increasing the glucose concentration in the water compartment (diffusion process driven by a concentration gradient).

Fick's first law (Eq. 5) was applied to obtain the results of glucose diffusivity with diffusion cell under the assumption of steady state conditions:

$$J_D = -D_{gluc} \cdot \frac{\Delta C}{\delta} \quad (5)$$

Where J_D is the glucose diffusion flux ($\text{g m}^{-2} \text{s}^{-1}$), D_{gluc} is the diffusion coefficient or diffusivity, ΔC is the concentration gradient (g m^{-3}) and δ is the diffusion length, in this case the thickness of the membrane (m). The development and calculus done to determine D_{gluc} could be seen in *Appendix F: Glucose diffusivity results*.

The effective diffusion of glucose D_{gluc} obtained experimentally was $4.00 \cdot 10^{-10} \pm 1.46 \cdot 10^{-10} \text{ m}^2 \text{s}^{-1}$. The molecular glucose diffusion in water ($D_{m,gluc}$) was found to be $6.90 \cdot 10^{-10} \text{ m}^2 \text{s}^{-1}$ at 25°C [35] and $9.00 \cdot 10^{-10} \text{ m}^2 \text{s}^{-1}$ at 37°C [36]. A relationship that takes into account the diffusive mass transport through the scaffold is summarized in Eq. 6 [9]:

$$Def f = \frac{D_m \cdot \varepsilon}{\tau} \quad (6)$$

Where the porosity (ε), and the tortuosity (τ) of the membrane are considered.

The PCL/rGO membrane has a reported porosity of 0.80 [8]. Applying an empirical relationship (Eq. 7) [9], the tortuosity for these membranes was 1.21.

$$\tau^2 = 1 - \ln(\varepsilon^2) \quad (7)$$

By using the value of the $D_{m,gluc}$ at 25°C, a value of $D_{gluc,eff} = 4.56 \cdot 10^{-10} \text{ m}^2 \text{s}^{-1}$ was obtained very proximate to our experimental data.

Comparing the diffusivity obtained with other studies (Table 3.2), the glucose diffusivity in these PCL/rGO membranes is the highest one reported. Relating PCL and PCL/rGO scaffolds, Table 3.2 reflects that the glucose diffusion coefficient is higher in membranes that incorporated nanoparticles of rGO. This is because membranes containing graphene oxide-based nanoplatelets had larger pores than the pristine PCL membranes [8], knowing that the effective diffusion coefficient is higher for a material with larger pore size [9]. The PVDF membrane had the smaller $D_{gluc,eff}$ as it presented the tinier pore size.

3. RESULTS AND DISCUSSION

Table 3. 2. Comparison of effective diffusion coefficients for glucose across typical TE scaffolds saturated in water

Membrane material	Temperature (°C)	$D_{\text{gluc, eff}}$ ($10^{-10} \text{ m}^2 \text{ s}^{-1}$)	Reference
PCL/rGO	25	4.00 ± 1.46	Present work
PCL	27	3.52 ± 2.35	Suhaimi [9]
PLLA	27	2.08 ± 0.20	Suhaimi [9]
5 wt% PLLA in dioxane solution ($\delta = 52 \text{ } \mu\text{m}$)	37	0.15 ± 0.05	Papenburg [36]
5 wt% PLLA in dioxane solution ($\delta = 21 \text{ } \mu\text{m}$)	37	1.04 ± 0.45	Papenburg [36]
PVDF	27	1.20 ± 0.38	Suhaimi [9]

Besides, an important factor that could be studied is the thickness of the membrane and the temperature. With lower thickness and higher temperatures the diffusion coefficient is higher because of the lower resistance to the diffusion transport.

The characterized membranes were asymmetric with large pores in the lower part and small pores in the upper part. The high diffusion values obtained in comparison with the other membranes may also be due to the fact that the effective thickness was much lower than the overall thickness measured in the present PCL/rGO membranes. Obviously, as it has been seen, temperature influences. Therefore, it should be taken into account for future studies.

3.2. OXYGEN SENSING SYSTEM RESULTS

It has been seen that the equipment needed a stabilization time to start the measurement, normally the first measurement was 0 mg O₂/L that had to be discarded.

Figure 3.3 presents the O₂ concentration monitored with time on the alimentation tank in experiments performed at 37°C. The O₂ concentration observed was always constant at 7.1 mg O₂/L, similar to typical reported levels of dissolved oxygen in fresh water at 37°C (6.8 mg O₂/L) [37]. The highest concentration of oxygen corresponded to the deionized water, around 7.5 mg O₂/L and tap water had an approximate value of 6.9 mg O₂/L, in consistence with the reduction of O₂ solubility on salt solutions [38], which means that the measurement is reliable.

Also, the temperature and atmospheric pressure are important variables in the system because at higher temperatures and lower pressures, the dissolved oxygen content is lower.

By introducing recirculation into the system, the dissolved oxygen content in water was slightly increased (for example, in distilled water from 7.40 to 7.54 mg O₂/L) due to the aeration through the silicone tubes used for pumping. In addition, the system gave similar values both in continuous and discrete measurements, benefiting continuous oxygen data collection in the BR (see *Appendix G: Continuous and discrete measurements of oxygen*).

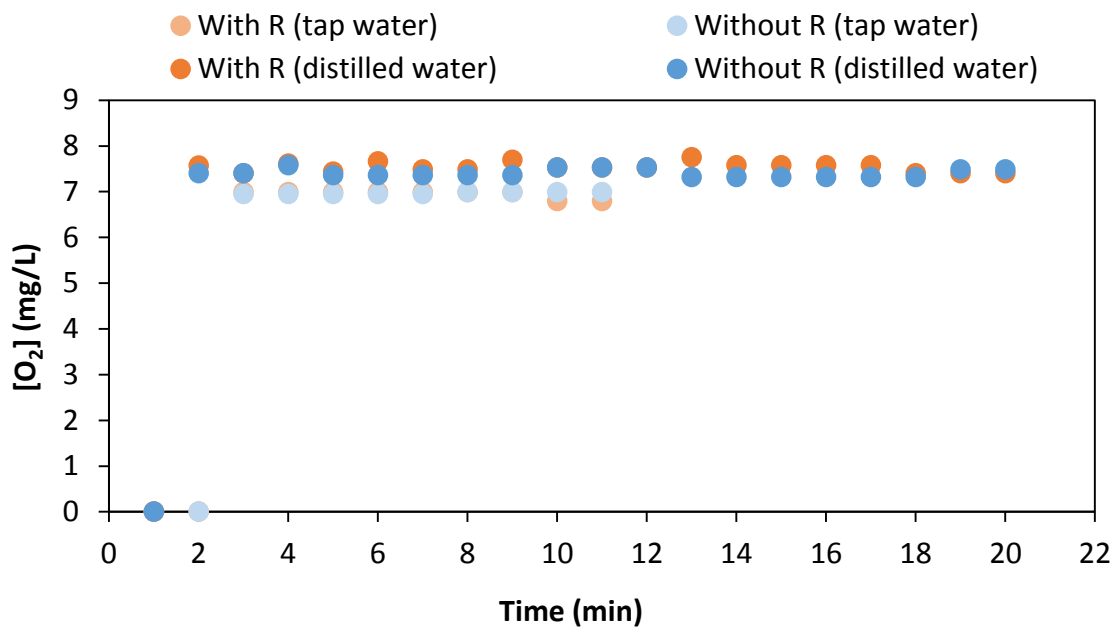


Figure 3.3. Oxygen concentration in water for tap water, distilled water and UP water, with and without recirculation

Once the reliability of the oximeter was verified, an exhaustive analysis was carried out for monitoring the O₂ content during the dynamic cell culture with Dulbecco's-modified Eagle's medium which is the frequent medium used in the culture of glioblastoma neural cells.

The average oxygen concentration in the cell chamber of the BR was 6.57-6.74 mg O₂/L during all the time period of the experiment. The typical value of oxygen concentration in various mediums under cell culture conditions had been reported to be 6.40-7.04 mg O₂/L [25], which corresponds with the values obtained during this work. Although certain oxygen consumption by the cells was observed, this concentration was still

sufficient to meet the demands of oxygen by the cells, and therefore oxygen could not been considered a limiting nutrient in the system under the present conditions tested. Additional data regarding the dynamic cell culture experiment could be found in *Appendix D: Dynamic cell culture*.

3.3. EXPERIMENTAL SETUP DATA

Preliminary tests developed with water in the perfusion BR system with tangential flow reflect that not fouling appear in the PCL/rGO membranes, with a constant permeate flux around $25 \text{ L m}^{-2} \text{ h}^{-1}$ at 0.03 bar. With the cross-flow filtration system used to characterize the membrane and the adjustment done (Figure 3.1), the membrane gave a permeate flux of $30 \text{ L m}^{-2} \text{ h}^{-1}$ at a pressure of 0.03 bar confirming similar membrane performance in both systems.

Figure 3.4 shows the change with time of total permeate flux of a model solution of BSA and glucose dissolved in PBS at 37°C with replicates performed at 1 mL min^{-1} and 8.5 mL min^{-1} . Thus, the influence of the inlet flowrate in the system was analyzed.

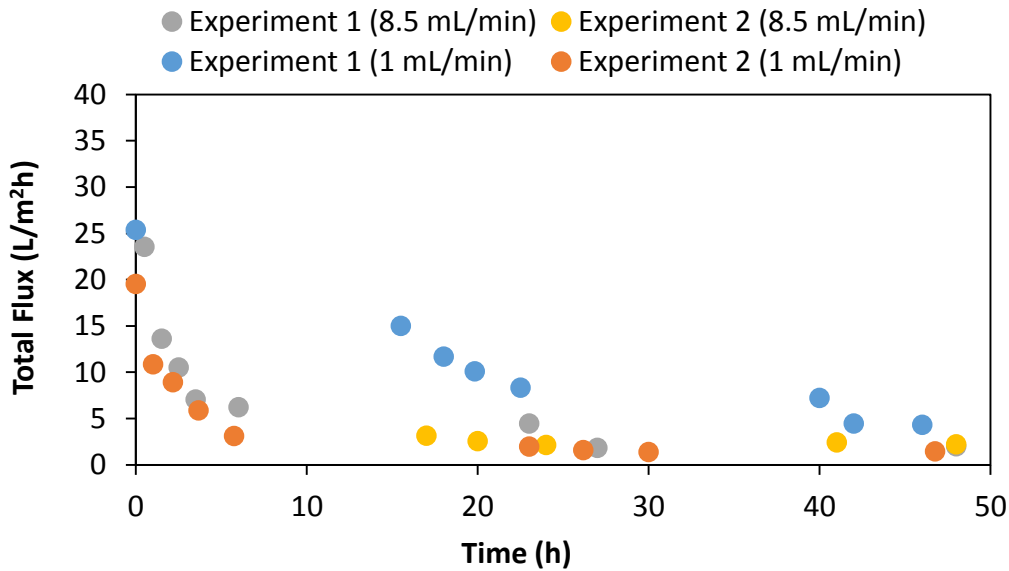


Figure 3. 4. Total permeate flux for experiments at different inlet flowrates (zoom).

Independently of the initial flowrate, all the experiments showed similar fouling behavior and reached similar steady-state fluxes.

The Reynolds number [39] was analyzed to understand better the results for different inlet flowrates. *Appendix H: Reynolds number calculation* shows the equations under the supposition of flow of non-compressible fluids (PBS) in pipes and raceways. Reynolds number were 1.47 and 12.5 at 1 and 8.5 mL min⁻¹ respectively, always below 2100 [39] in both flowrates for the present configuration of the perfusion cell, indicating laminar flowrate regime. The change in flowrate under the maximum and minimum flowrate conditions that the pump supplies, does not affect the mass transport through the membrane. Therefore, it can be considered an overall mass transport kinetic parameter in the membrane including concentration polarization phenomena for the present system.

The fitting of the experimental data to several different fouling models were evaluated. Parameters fitting are shown in Table 3.3:

Table 3. 3. *Fouling mechanisms adjustment*

Fouling mechanism	Parameters adjusted	Coeficiente de ajuste
Cake layer	$\alpha f = 1.67 \cdot 10^{14}$	$R^2 = 0.66$
Complete blocking	$a = -0.07$ $b = 0.16$	$R^2 = 0.73$
Intermediate blocking	$a = 11.06$ $b = 39.39$	$R^2 = 0.80$
Combined model	$\alpha = 25.5$ $R_{f0} = 6.94 \cdot 10^{13}$ $\beta = 2.4 \cdot 10^{12}$	% of variation (ACM)=76.7

The parameters of the model combining initial internal fouling and final cake formation were estimated in ACM. A sensitivity analysis of the influence of the values of β demonstrated that this parameter barely influenced in the simulated data, so the value of $2.4 \cdot 10^{12}$ was fixed according to what it was reported by Ho and Zydney [22] for the fouling of microfiltration membranes with BSA. The resistance of the initial protein deposit (R_{f0}) were estimated from the Kozeny-Carman equation as:

$$R_{f0} = \frac{5 \cdot \delta}{\varepsilon \cdot S^2} \quad (8)$$

Adapting Eq. 8 for the PCL/rGO scaffold with $\delta = 100 \mu\text{m}$, $\varepsilon = 0.8$ and S , the specific surface area of the protein BSA deposit was $30 \cdot 10^{-10} \text{ m}^2$ [22]. R_{f0} indicates the rate of blockage of the pore.

The α value was estimated and had a value of $25.5 \text{ m}^2 \text{ kg}^{-1}$. That is an order of magnitude higher than the average value reported (4.1) by Ho and Zydney [22]. The PCL/rGO membranes had an average pore size of approximately $0.6 \text{ }\mu\text{m}$, much larger than the membranes used in the article ($0.22 \text{ }\mu\text{m}$). In addition, in the present work the model feed solution was not pre-filtered to remove larger aggregates. Therefore, the α value obtained for the PCL/rGO membranes is plausible.

Figure 3.5 represents the experimental data of 4 experiments and the fitting to the different models.

3. RESULTS AND DISCUSSION

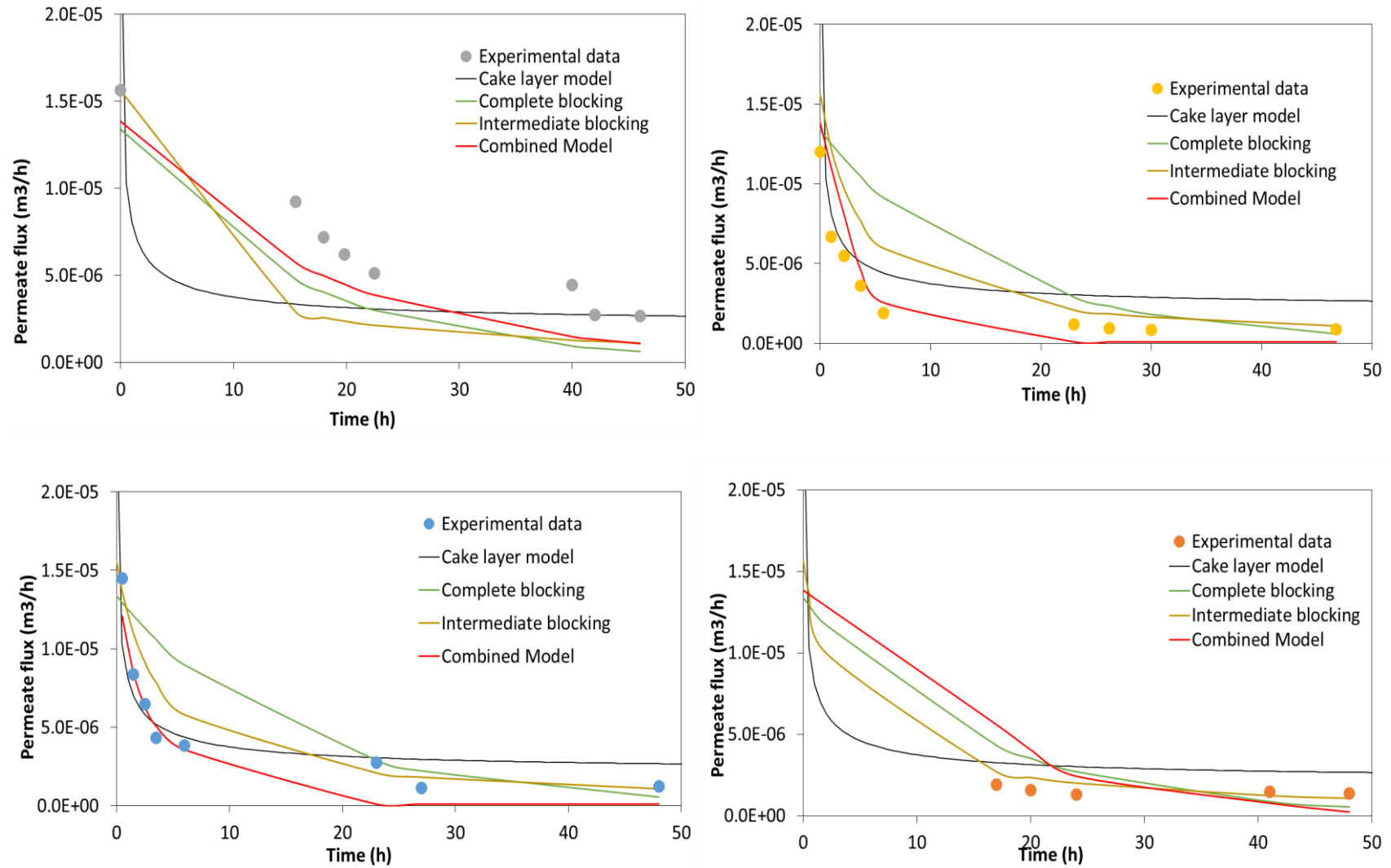


Figure 3. 5. Experimental data at different feed flowrates (1 and 8.5 mL min⁻¹) fitted with the different models proposed

With the models presented in Figure 3.5, it could be seen that the model which best adjusted the all the experimental data is the combined model. It means that the fouling mechanism comes from adsorption of BSA protein into the pores and later a cake layer formation.

Overall, although the cake formation model did not fit all the experiments individually, Figure 3.6 shows that this model represents a realistic approximation of the average behavior of the membrane fouling performance being valid simplification for subsequent modelling analysis.

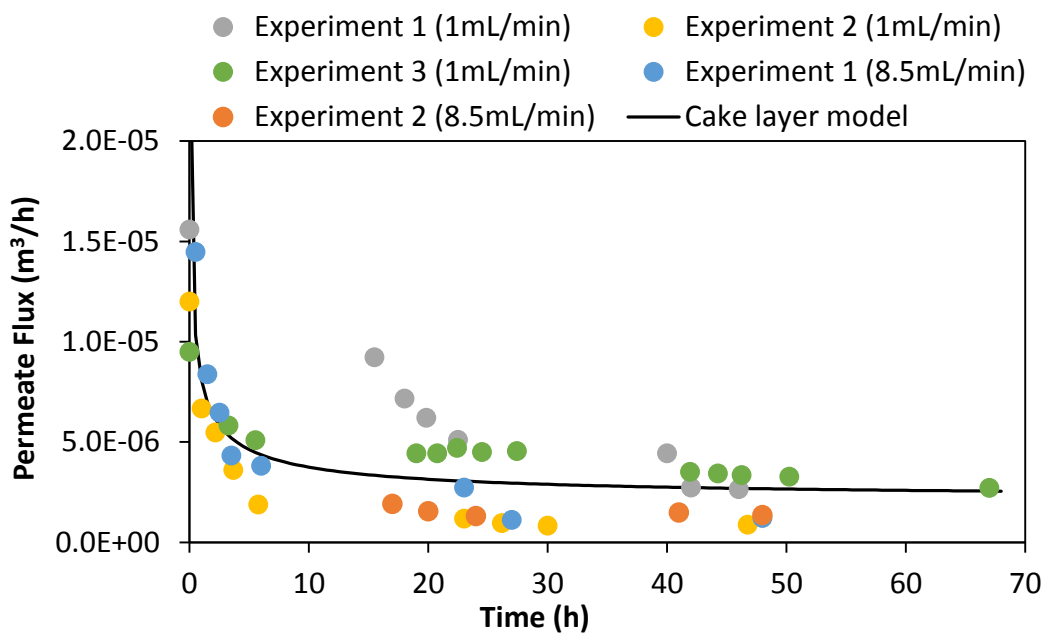


Figure 3. 6. Progression of permeate flowrate with time for experimental data and model developed.

The transmittance of the BSA protein and glucose nutrient through the membrane was analyzed as well. It is necessary to control these variables to guarantee the feeding of the cells supported in the membrane and their growth if there were. The ratio of nutrient and protein transmission was calculated by Eq. 9:

$$\% \text{ Transmission} = T_r = \frac{C_p}{C_f} \cdot 100 \quad (9)$$

Where C_p and C_f are the BSA or glucose concentrations in the permeate and in the feed solutions.

Figure 3.7 shows the change in the transmittances of BSA with time. PCL/rGO membranes transmittances were in all cases between 50 and 100%. It could be seen that at first, the percentage of transmission for the protein was higher because membranes were cleaned and there was not fouling resistance, but with the increase of filtration time, the transmittance decreased due to the pore blockage and cake layer produced.

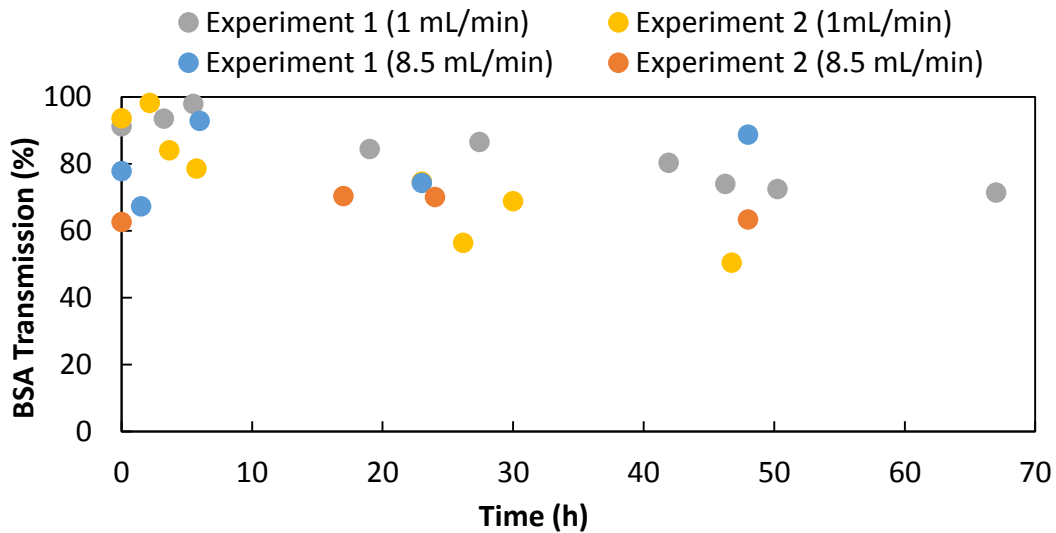


Figure 3. 7. Evolution of the protein transmission with time.

Figure 3.8 represents the evolution of the glucose transmission with time. In this case it can be seen that the transmission was maintained always constant between the ranges 80-100%. So, a high glucose supply to the cell compartment was ensured.

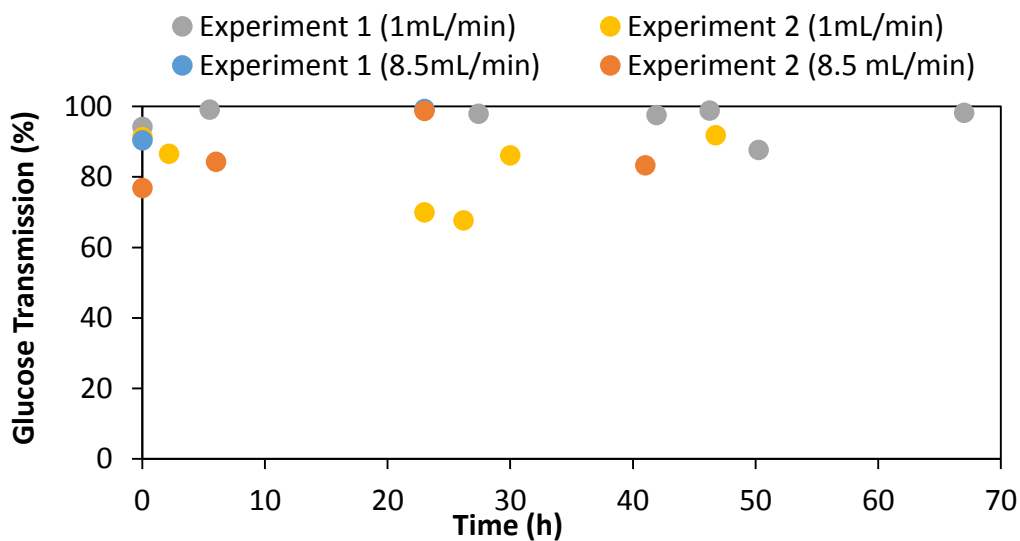


Figure 3. 8. Evolution of the glucose transmission with time.

In order to determine the influence of diffusion on the overall glucose flux through the membrane under perfusion conditions, a comparison of the glucose fluxes achieved by diffusion and convection were compared. The maximum diffusion flux obtained was $0.186 \text{ L m}^{-2} \text{ h}^{-1}$ and the minimum convective flux was $1.445 \text{ L m}^{-2} \text{ h}^{-1}$, which is 87.12% higher than diffusive flux. Hence, the convective flux of glucose is much higher than the diffusion one. Therefore, the mechanism of mass transport by diffusion can be disregarded assuming a simplified mathematical model.

3.4. MATHEMATICAL MODEL RESULTS

As it has been proved, the fouling mechanism in the PCL rGO membranes is given by a combination of the adsorption/deposition of BSA in the pores of the membrane and a subsequent formation of cake layer. However, as it has been already demonstrated before (Figure 3.6) the cake formation model describes sufficiently well the average behavior of the fouling of the membrane under the present working conditions, therefore, the following computational simulations for the cellular analysis will be done under this assumption to make a preliminary analysis of the parameters of influence, limiting nutrients, etc.

3.4.1. Analysis of parameters sensitivity

Volume of feed tank

One of the most important variables in the perfusion BR system is the volume of culture medium needed to develop the cell culture as it will determine the glucose content and lactate concentration in the cell compartment. In order to predict optimum medium volume to have sufficient analytical sensitivity for future cell experiments under the BR perfusion dynamic experiments, a sensitivity analysis of the volume of the feed tank has been addressed.

The initial culture medium volume in the feed tank was varied from 30-100 mL. 30 was fixed as minimum volume because 10 mL were the less volume used as sampling to monitoring the experiments during time. Moreover, 15 mL of dead volume was in the

system. So, 30 mL is the more restrictive value. And 100 mL, was selected to see the comparison with much higher culture medium volumes.

For the simulations we considered neural progenitor cells (NPC) proliferation rate attained from previous experiments performed in the TAB group [11]. Other biological variables like glucose consumption by cells or lactate production not changed with the change of volume. These biological parameters were not known for NPCs. Therefore other parameters from different cellular systems were used for the simulations.

In Figure 3.9, the variation of the concentration of glucose in the cellular chamber is shown. A progressive decrease of glucose in the cellular chamber was observed at any feed volume. It is observed that after 5 days of culture, using 30 mL of feed volume only a final concentration of $0.24 \text{ kg glucose m}^{-3}$ was left. That means that with an initial volume of 30 mL, the cells did not have deficit of the main nutrient to proliferate and growth.

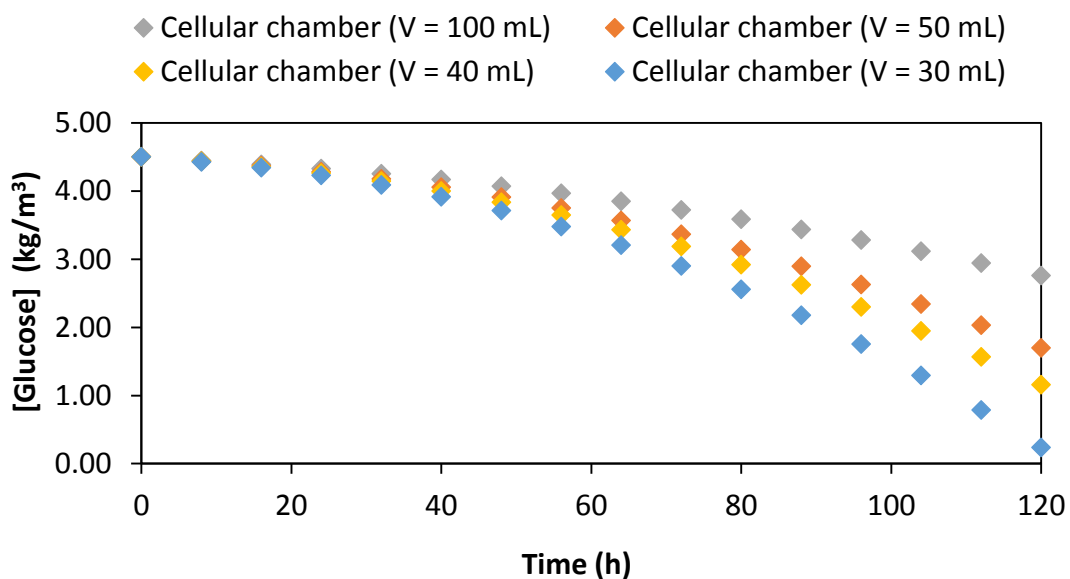


Figure 3. 9. Variation of glucose concentration in cellular chamber for different initial culture medium volume

In Figure 3. 10 the variation of lactate concentration is shown. In this case, the lactate concentration in the cellular chamber increases progressively as expected. Besides, the higher the initial feed volume the lower the lactate concentration is observed due to its higher dilution on the feed tank. Multiple studies have shown that the presence of lactate in cell culture restricts cell growth in concentrations above 3.6 kg m^{-3} [40]. With

a volume of 30 mL 3.11 kg lactate m⁻³ were produced. This value was near that the limit value which restricted cell growth and have to be considered.

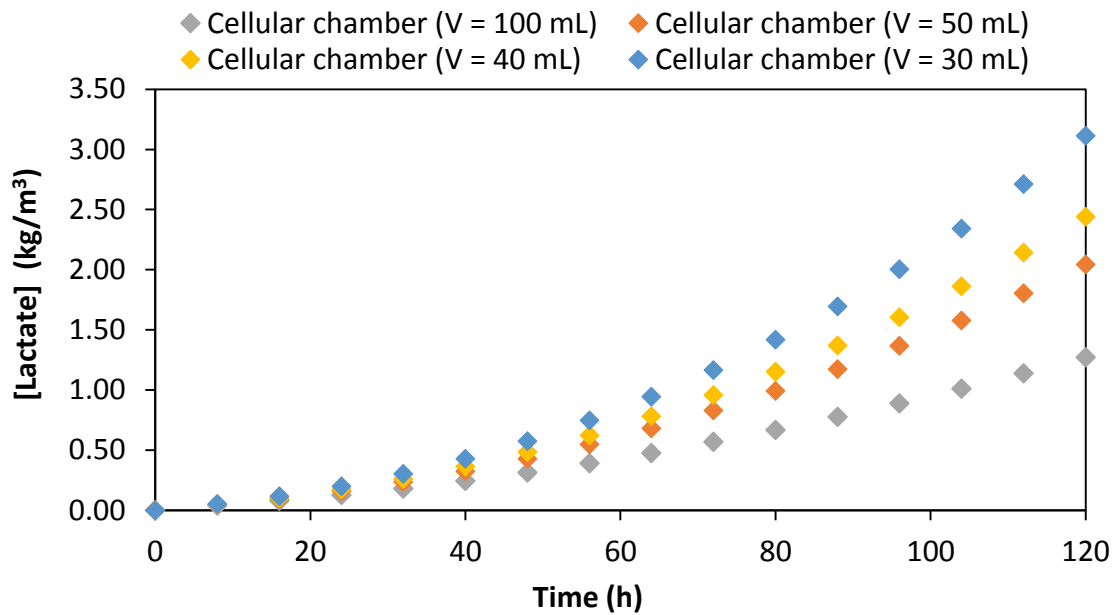


Figure 3. 10. Variation of lactate concentration in cellular chamber for different initial culture medium volume

The model predicted complete consumption of glucose for low feed tank volumes, whereas depletion of oxygen in the cellular chamber did not occur (Figure 3.11), due to continuous replenishment of oxygen into the feed tank and therefore in the vascular chamber. There was a decrease in the concentration of oxygen with time due to the higher cell population at 5 days as expected, but the O₂ level was still in the water saturation values.

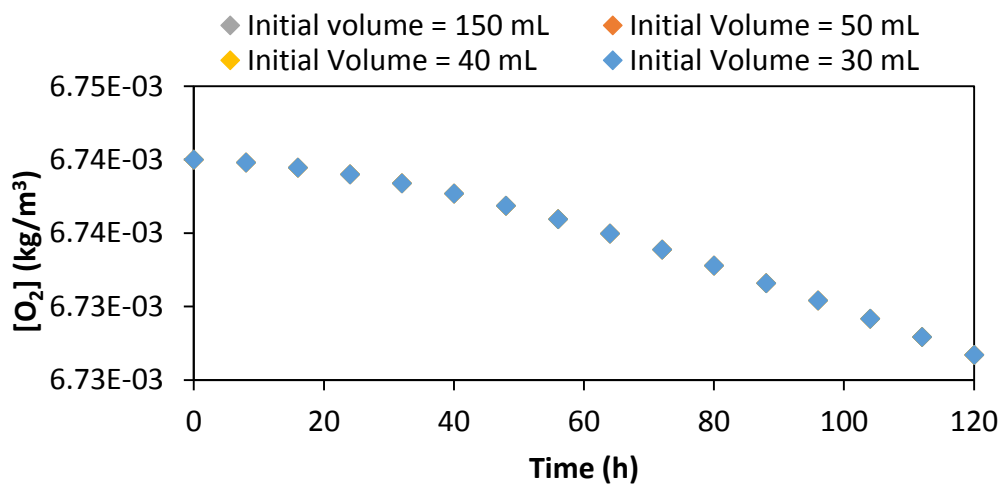


Figure 3. 11. Variation of oxygen concentration in cellular chamber for different initial culture medium volume

In view of the results, the use of an initial feed tank volume of culture medium of 30 mL would be sufficient for future experiments of perfusion BR with cells. However, this would imply that a 50% of the total feed volume is contained in the tubes and parts of the system. Therefore, the actual working volume should be increased up to at least 60 mL.

Cells growth kinetic parameters

Vero cells (kidney epithelial cells extracted from an African green monkey) are taken as a base in the sensitivity analysis done as well as in the mathematical model with cells. The analysis were done in the cellular chamber because is the limiting part in the system. The sensitivity analysis could be seen in *Appendix I: Cells growth kinetic parameters*.

From the present sensitivity analysis it can be concluded that high dependence of the nutrients consumption and metabolites production depending on the cellular type which ultimately depend on the biological kinetic parameters. The great uncertainty on these biological parameters for the present cellular type makes advisable to determine these coefficients experimentally for future works.

4. CONCLUSIONS AND FUTURE CHALLENGES

In this project it has been possible to advance in the objective of achieving the development of a neuronal model in the perfusion bioreactor system with biocompatible and biodegradable polymeric membranes of PCL/rGO.

The design and improvement of the system has been carried out. The assembly and tuning of the main elements of the perfusion bioreactor was made: pressure transducer, oxygen meter, perfusion cell, feed tank and peristaltic pump. The dead volume of the system was also minimized. Calibration and experimentation with the oximeter, as well as the mathematical model developed, allowed determining that the O_2 is not a critical nutrient in this system under the operating conditions carried out, but it is an important nutrient to monitor during cell culture.

Advances in the experimental and mathematical description of the fouling phenomena in the present PCL/rGO microfiltration membrane were done. The experimental data were fitted to different fouling models and the most convenient mathematical description was found to be a combined model that included initial stages of pore blockage and final stages of cake formation. However, the cake formation model could satisfactorily describe the average fouling mechanism for a mathematical model simplification.

The transmittance of BSA and glucose through has been analyzed as well as the coefficient of effective diffusion of the glucose through the membrane of PCL/rGO. This values confirmed high convective transport of nutrients and negligible influence of diffusion mechanisms for glucose.

In addition, a novel mathematical model was developed to describe the nutrients supply, metabolites formation and cell growth and proliferation through a perfusion BR using a flat membrane scaffold. The main novelty of the model was including a fouling mechanism that importantly affected the nutrients supply in the initial cell proliferative stages. The mathematical model developed served to demonstrate the feasibility of growing different cellular types in this system and to determine the adequate volume of the feed tank to explore future experiments with cell under dynamic culture conditions with the present perfusion BR. Also the importance to retrieve the specific NPC yield parameters defined in the Monod expression has been remarked.

For future work, a specific analysis of the variation of the concentration of BSA with experimental time is proposed to integrate it into the defined fouling mechanism. In addition, specific experiments will be planned in dynamic cell culture to determine the real kinetic parameters for neural cells.

Finally, implementing a system in CFD is another of the future tasks to describe not only the variation of nutrients in the cell culture but also the physical forces that can cause cellular stress.

5. REFERENCES

- [1]. IKADA, Y. 2006. Challenges in tissue engineering. *Journal of the Royal Society Interface*, **3** (10), pp. 589-601. ISSN: 1742-5689.
- [2]. LANGER, R.; VACANTI, J.P. 1993. Tissue Engineering. *Science*, **260** (5110), pp. 920-6. ISSN 0036-8075.
- [3]. DIBAN N. STAMATIALIS D.F. 2014. Polymeric hollow fiber membranes for bioartificial organs and tissue engineering applications. *Society of Chemical Industry*, **89** (5), pp. 633-643.
- [4]. PÖRTNER, R. [et al.]. 2005. Bioreactor design for tissue engineering. *Journal of Bioscience and Bioengineering*, **100** (3), pp. 235–245. ISSN: 1389-1723.
- [5]. STAMATIALIS, D.F. [et al.]. 2007. Medical applications of membranes: Drug delivery, artificial organs and tissue engineering. *Journal of Membrane Science*, **308** (1-2), pp. 1–34.
- [6]. SALEHI-NIK, N. [et al.]. 2013. Engineering parameters in bioreactor's design: a critical aspect in tissue engineering. *Biomed Research International*, **1** (9), pp. 1-15. ISSN: 2314-6141.
- [7]. DIBAN, N. 2014. Perspectives on engineering organs in vitro: overcoming oxygen supply limitations. *Journal of Chemical Engineering Research Studies*, **1** (2). ISSN: 2394-1154.
- [8]. DIBAN, N. [et al.]. 2017. Facile fabrication of poly (ϵ -caprolactone)/graphene oxide membranes for bioreactors in tissue engineering. *Journal of Membrane Science*, **540**, pp. 219-228.
- [9]. SUHAIMI, H. 2015. *Glucose Diffusivity in Tissue Engineering Membranes and Scaffolds: Implications for Hollow Fibre Membrane Bioreactor*. Doctoral Thesis, Loughborough University.
- [10]. LADEWIG, B. AL-SHAELI, M. 2016. *Fundamentals of Membrane Bioreactors. Materials, Systems and Membrane Fouling*. Transactions in Civil and Environmental Engineering. Springer.
- [11]. SANCHEZ-GONZALEZ, S. [et al.]. 2018. Hydrolytic Degradation and Mechanical Stability of Poly (ϵ -Caprolactone)/Reduced Graphene Oxide Membranes as Scaffolds for In Vitro Neural Tissue Regeneration. *Membranes*, **8** (1), pp. 12-26. ISSN: 2077-0375.

- [12]. SEAN, K., ANDREW, Z. 1995. Mechanisms for BSA fouling during microfiltration. *Journal of Membrane Science*, **107** (1–2), pp. 115-127.
- [13]. IVANOVIC, Z. 2009. Hypoxia or in situ normoxia: the stem cell paradigm. *Journal of Cellular Physiology*, **219** (2), pp. 271–5.
- [14]. FASSNACHT, D. AND PÖRTNER, R. 1999. Experimental and theoretical considerations on oxygen supply for animal cell growth in fixed bed reactors. *Journal of Biotechnology*, **72**, pp. 169–184.
- [15]. HAY, P.D. [et al.]. 2000. Oxygen Transfer in a Diffusion-Limited Hollow Fiber Bioartificial Liver. *International Society for Artificial Organs*, **24** (4), pp. 278-288.
- [16]. YAN, X. 2011. *MODELING OF MASS TRANSFER AND FLUID FLOW IN PERUFUSION BIOREACTORS*. Doctoral Thesis, University of Saskatchewan.
- [17]. CHAPMAN, L. 2017. Mathematical modelling of cell layer growth in a hollow fibre bioreactor. *Journal of Theoretical Biology*, **418**, pp. 36-56.
- [18]. PAPE, A. [et al.]. 2017. Cell and Protein Fouling Properties of Polymeric Mixtures Containing Supramolecular Poly(ethylene glycol) Additives. *Langmuir*, **33** (16), pp. 4076-4082.
- [19]. DIBAN, N. [et al.]. 2013. Effect of Surface Morphology of Poly(ϵ -caprolactone) Scaffolds on Adipose Stem Cell Adhesion and Proliferation. *Wiley-VCH, Macromolecular Symposia*, **334**, pp. 126-132.
- [20]. CASTROS, P. [et al.]. 1995. CHO cell growth and recombinant Interferon- γ production: Effects of BSA Pluronic and lipids. *Cytotechnology*, **19** (1), pp. 27-36.
- [21]. YE, Y. [et al.]. 2005. Fouling mechanisms of alginate solutions as model extracellular polymeric substances. *Desalination*, **175**, pp. 7-20.
- [22]. HO, C. ZYDNEY, A. 2000. A Combined Pore Blockage and Cake Filtration Model for Protein Fouling during Microfiltration. *Journal of Colloid and Interface Science*, **232**, pp. 389-399.

- [23]. ROUWKEMA, J. [et al.]. 2009. Supply of Nutrients to Cells in Engineered Tissues. *Biotechnology and Genetic Engineering Reviews*, **26** (1), pp.163-178.
- [24]. HUCHZERMEYER, C. [et al.]. 2013. Oxygen consumption rates during three different neuronal activity states in the hippocampal CA3 network. *Journal of Cerebral Blood Flow & Metabolism*, **33**, pp.263-271.
- [25]. MCMURTREY, R. 2016. Models of Oxygen and Nutrient Diffusion, Metabolism Dynamics, and Architecture Optimization in Three-Dimensional Tissue Constructs with Applications and Insights in Cerebral Organoids. *Tissue Engineering*, **22** (3), pp. 221-249.
- [26]. BOUDRANTA, J. [et al.]. 2005. Mathematical modelling of cell suspension in high cell density conditions Application to L-lactic acid fermentation using *Lactobacillus casei* in membrane bioreactor. *Process Biochemistry*, **40**, pp. 1641-7.
- [27]. URSACHE, R. 2014. Mathematical model of adherent Vero cell growth and poliovirus production in animal component free medium. *Bioprocess Biosyst Eng*.
- [28]. CRAVEN, S. WHELAN, J. GLENNON, B. 2014. Glucose concentration control of a fed-batch mammalian cell bioprocess using a nonlinear model predictive controller. *Journal of Process Control*, **24**, pp. 344-357.
- [29]. Fluxion Biosciences, Inc. 2008. Technical note. *Viscosity. Understanding effects of viscosity in the BioFlux system*. Available at: https://support.fluxionbio.com/hc/en-us/article_attachments/200977338/bioflux_viscosity_technote-1038-01.pdf [Accessed: 25/06/2017].
- [30]. PHILLIPS, K. [et al.]. 2012. Measurement of single cell refractive index, dry mass, volume, and density using a transillumination microscope. *Physical Review Letter*, **109** (11).
- [31]. GENTET, L. 2000. Direct Measurement of Specific Membrane Capacitance in Neurons. *Biophysical journal*, **79**, pp. 314-320.
- [32]. DIBAN, N. [et al.]. [2013]. Development and characterization of poly(ϵ -caprolactone) hollow fiber membranes for vascular tissue engineering, *Journal of Membrane Science*, **438**, pp. 29-37.

- [33]. Bettahalli, N.M.S. 2011. Development of poly(L-lactic acid) hollow fiber membranes for artificial vasculature in tissue engineering scaffolds. *Journal of Membrane Science*, **371**, pp. 117-126.
- [34]. DE BARTOLO, L. [et al.]. 2007. Human lymphocyte PEEK-WC hollow fiber membrane bioreactor. *Journal of biotechnology*, **132** (1), pp. 65-74.
- [35]. PERRY, R. [et al.]. 1984. *Perry's chemical engineers' handbook*. 6th ed. New York: McGraw-Hill.
- [36]. PAPENBURG, B. 2009. Design strategies for tissue engineering scaffolds. Doctoral thesis, University of Twente, Holanda.
- [37]. Engineering ToolBox. 2005. *Oxygen - Solubility in Fresh Water and Sea Water*. [Online]. Available at: https://www.engineeringtoolbox.com/oxygen-solubility-water-d_841.html [Accessed: 9/07/2018].
- [38]. PEÑA, E. 2007. Calidad de agua. Trabajo de investigación oxígeno disuelto. Higher Polytechnic School of the Litoral. Engineering in Audit and Management Control.
- [39]. MCCABE, W.; SMITH, J.; HARRIOT, P. 2001. *Operaciones Unitarias de Ingeniería Química*. 6a. ed. New York, USA. McGraw – Hill.
- [40]. MARTINEZ, V. 2007. Optimización del Cultivo de Células HEK293 en Suspensión para su Crecimiento y Producción de Adenovirus. Doctoral Thesis. Santiago de Chile, University of Chile.

6. APPENDIX

Appendix A: Peristaltic Pump Calibration

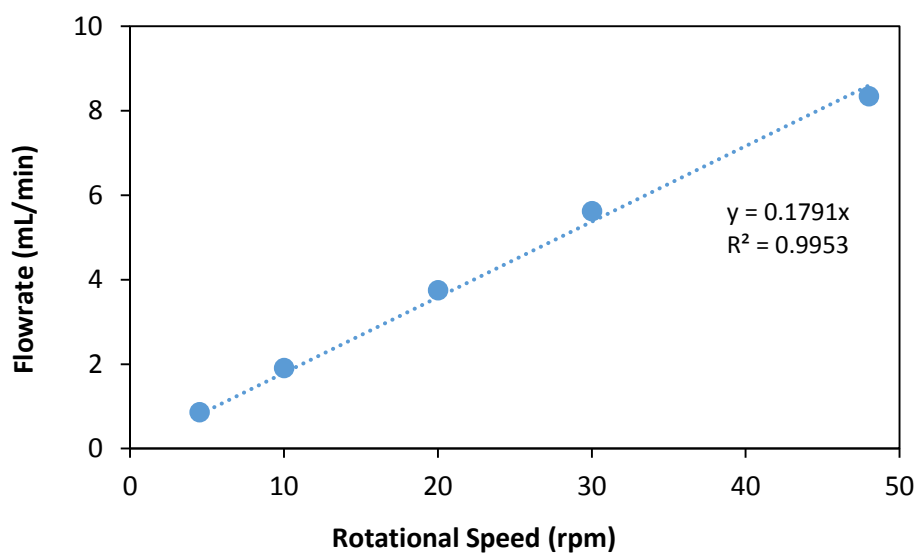


Figure 6. 1. Calibration line of the Peristaltic Pump-MINIPULS 3

Appendix B: Cross-flow filtration setup



Figure 6. 2. Homemade cross-flow filtration system

Appendix C: Glucose and lactate quantification protocols

Glucose

The "GLUCOSE GOD-PAP, BIOLABO" lab kit was used to quantify glucose. The steps to follow are:

1. Put the reagents and samples at room temperature.
2. Prepare the blank, standard and different samples in test tubes, as follows:
 - a. Blank: 1 mL of the reactive 1 (buffer solution) + 10 μ L of distilled water.
 - b. Standard: 1 mL of the reactive 1 (buffer solution) + 10 μ L of reactive 2 (standard of 1 g/L of glucose).
 - c. Sample: 1 mL of the reactive 1 (buffer solution) + 10 μ L of sample.
3. Mix well.
4. Incubate at 37 °C during 10 min.
5. Read the absorbance at 500 nm against the blank reactive. The coloration is stable during 15-20 min, later it decreases slowly.
6. Calculation of glucose, Eq. A1:

$$\text{Glucose (g/L)} = \frac{\text{ABS sample}}{\text{ABS standard}} \cdot \text{Concentration of standard (1g/L)} \quad (\text{A1})$$

Apart from the equation described above, a calibration line with different concentrations of glucose was done in order to check the method.

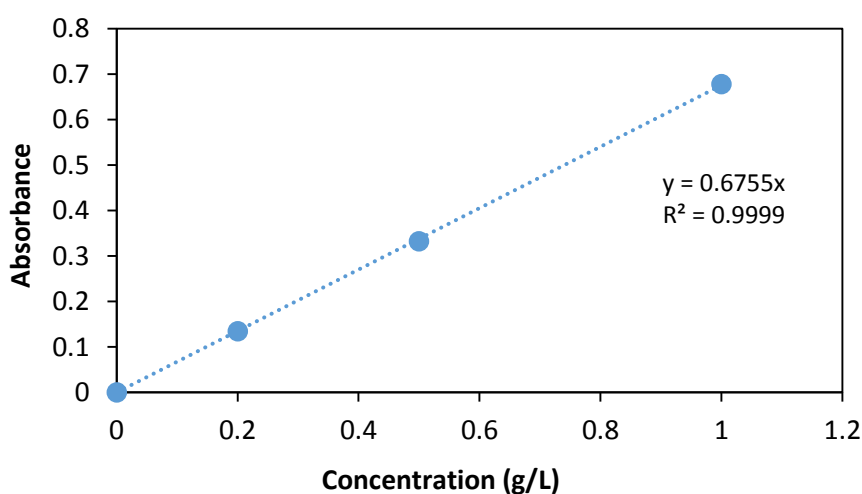


Figure 6.3. Calibration line of glucose concentration from absorbance UV

Lactate

The "LACTATE (LIQUID) REAGENT SET, POINTE SCIENTIFIC, INC." lab kit was used to quantify lactate. The steps to follow are:

1. Put the reagents and samples at room temperature.
2. Prepare the blank, standard and different samples in test tubes, as follows:
 - Add 300 μL of the reagent 1 (buffer solution) + 6 μL of sample. Put it at 37°C during 30 seconds.
 - Next, add 200 μL of the reagent 2 (buffer solution). Put it at 37°C during 5 min.

For the blank, the sample is distilled water, for the standard the sample is the lactate standard (5mmol/L) and finally, for measuring the concentration of the samples each sample is measured.

3. Read the absorbance at 550 nm against the blank reactive.
4. Calculation of lactate concentration, Eq. A2:

$$\text{Lactate } \left(\frac{\text{g}}{\text{L}} \right) = \frac{\text{ABS sample}}{\text{ABS standard}} \cdot \text{Concentration of standard (0.45g/L)} \quad (\text{A2})$$

The assay range in which the lab kit is reliable is between 0-15 mmol of lactate per liter.

Appendix D: Dynamic cell culture**Experimental methodology**

The U87 human glioblastoma cell line (ATCC® HTB-14TM), which are brain tumor cells, was selected and maintained in Dulbecco's-modified Eagle's medium (DMEM, Gibco Invitrogen, USA) which is the usual medium used in the culture of glioblastoma neural cells in tissue engineering. The medium was supplemented with 10% of FBS and antibiotic agents (penicillin G, 100 U mL⁻¹ and streptomycin, 100 mg mL⁻¹) in a humidified atmosphere of 5% carbon dioxide and 95% air at 37°C (New Brunswick Galaxy S Series 170 S incubator).

The cells were trypsinized from culture flasks, resuspended in culture medium, and seeded uniformly onto the membranes at a cell density of 25000 cells cm⁻².

First, the membranes of the perfusion cell had been sterilized in ethanol, opening the pores, and later they were immersed in PBS to remove the traces of ethanol that could damage the cells.

Perfusion cell BRs containing the membranes and cells were kept in a humidified atmosphere of 5% carbon dioxide and 95% air at 37°C and incubated for 3h (to see the adherence of the cells; static conditions) and for 7 days (to see the proliferation of the cells; dynamic conditions).

100 mL of culture medium were put in the feeding tank. The medium was pumped at 9 rpm. The total permeate flux (Figure 6.4) and the oxygen concentrations during the evolution of the cell culture were measured. It was seen that the pressure in the system increased because of membrane bulging (in this system it was not used the pressure transmitter).

After incubation, the cells were fixed in cold paraformaldehyde (3% in PBS) for 20 min at room temperature, permeabilized with Triton X-100 (0.1% in PBS) for 5 min at room temperature, and washed three times with PBS. Fluorescent-labelled phalloidin (Atto-590, Sigma Aldrich, Spain), which interacted with the polymerized factin, was used to identify the actin filaments and fibres. NucBlue (Molecular Probes) was also used to stain the nuclei.

During microscopy observation, the membranes were inverted, and a series of optical sections (Figure 6.5) were obtained with a Nikon A1R confocal scanning laser microscope.

This test was carried out in the Microbiology Service of the IDIVAL Health Research Institute of the Marqués de Valdecilla Hospital.

Results

In Figure 6.4 it could be seen a drop in permeate flux during the first days due to fouling in the membrane and the cell layer on it. However, the permeate flux increased from day 4. This might indicate that the cells had detached from the membrane, as the confocal images at day 7 depict (Figure 6.5 b), and the resistance due to the cell layer was eliminated, increasing the permeate flux.

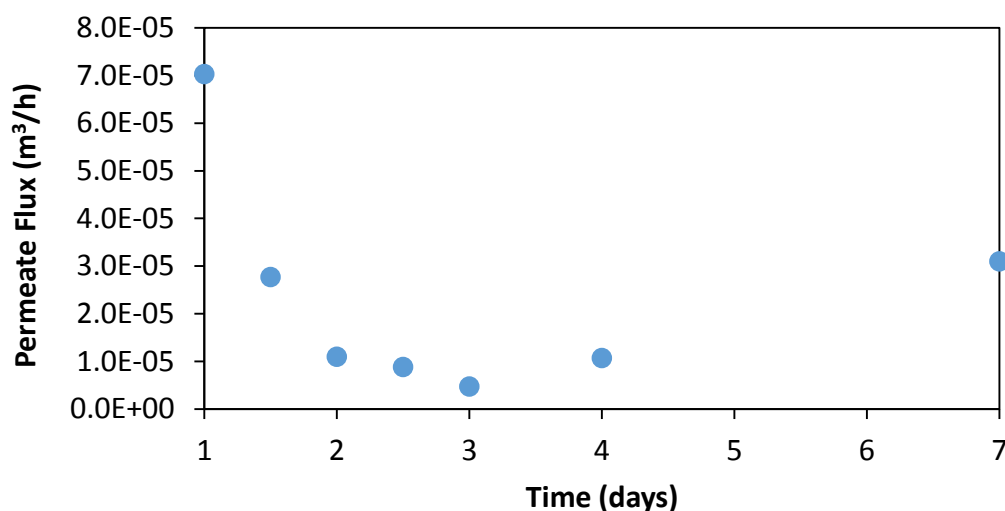


Figure 6. 4. Total permeate flux during the dynamic experiment

Figure 6.5 a) shows the good adherence of glioblastoma cells in the biocompatible PCL/rGO membrane at 3h of culture. In Figure 6.5 b) it could be seen that the cells detached from the membrane and disappeared.

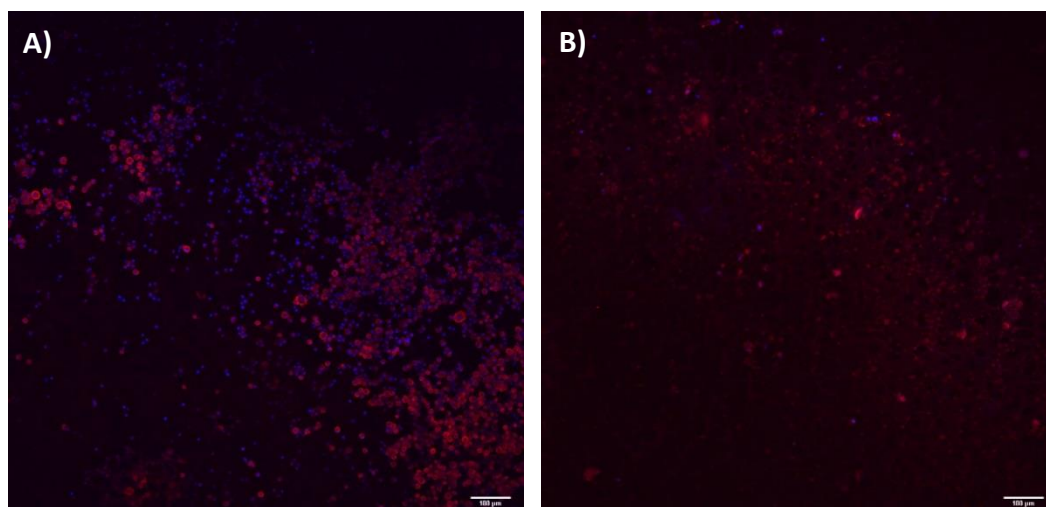


Figure 6. 5. Confocal microscopy images of the dynamic cell culture of the U87 cells on the PCL/rGO membranes at (a) 3 h and (b) 7 days

Because a lot of problems with tubing, leakages, tightness, and absence of cells at final of the experiment occurred, several test and improvements were made after that to get better the system for future cell cultures in dynamic conditions.

Appendix E: Mathematical model development

COMPLETE MODEL DEVELOPMENT

For the development of the mathematical model, it was important to define the nutrients and metabolites balances in the perfusion cell and feeding tank. The feeding tank and the vascular chamber had the same concentration of nutrients and metabolites due to the system configuration, so the total and component mass balances were developed only for the feeding tank and relating it with the vascular chamber.

1. Mass balances in the membrane

First, the balance of the permeate flux from the vascular chamber through the membrane to the cellular chamber for nutrients and metabolites (i) was developed, giving the Eq. A3, and considering both the scaffold and cell layer:

$$J_i = C_{i,v} \cdot \left(\frac{D_{i,eff}}{\delta} + \frac{D_{i,cell}}{x_{cell}} + K_{total} \cdot P \right) \quad (A3)$$

Where J_i is the flux mass transport contribution due to convection and diffusion mechanisms of i in $\text{kg m}^{-2} \text{h}^{-1}$, $C_{i,v}$ is the concentration of i in the vascular chamber in kg m^{-3} , $D_{i,eff}$ is the i effective diffusion coefficient across the PCL/rGO scaffold in $\text{m}^{-2} \text{h}^{-1}$, δ is the thickness of the membrane in m, x_{cell} is the thickness of the cell layer formed during the proliferation of U87 cells in m, K_{total} is the total permeability in the system with units of $\text{m}^3 \text{m}^{-2} \text{h}^{-1} \text{bar}^{-1}$ and finally, P is the average pressure obtained during the dynamic experiments in the system in bar.

2. Mass balances in the cellular chamber

Second, the mass balances in the cellular chamber for the nutrients (glucose in that case) and metabolite (lactate) was developed, giving the Eq. A4:

$$V_{cell} \cdot \frac{dC_{i,cell}}{dt} = J_i \cdot Am - Fp \cdot C_{i,cell} \pm r_i \quad (A4)$$

Where V_{cell} is the volume of the cellular chamber, $C_{i,cell}$ is the concentration of i in the cellular chamber, Fp is the permeate flux through the membrane in $\text{m}^3 \text{h}^{-1}$ and r_i is the term corresponding to substrate or product rate consumed or produced by cells in kg of i h^{-1} .

Third, the rates of substrate consumption and product formation (r_i) by cells and the Monod growth model for cells were described (Eq. A5, Eq.A6 and Eq.A7). The Monod equations were adapted to this system. To calculate the cell growth rate, the model of growth considered was one obtained experimentally in static cell culture conditions of human neural progenitor cells. For that:

$$\text{Cells number} = -14.12 * t^2 + 4919.4 * t + 57000 \quad (\text{A5})$$

At the initial of the static experiment, 57000 human neural progenitor cells were cultured, and in the next 5 days proliferates giving the relationship shown with time, by fitting experimental data to a polynomic adjusted line.

The glucose consume expressed as a rate was equal to:

$$-\frac{dC_{gluc}}{dt} = \text{Gluc consume} = \text{Cells number}(t) \cdot \text{masscell} \cdot (1/Y_{XS} + m) \quad (\text{A6})$$

Y_{XS} is the yield coefficient which represents the amount of cell in kg per amount of glucose in kg. It considered only consumption of substrate for growth purposes. In the other case it was m , the maintenance coefficient thus denotes extra substrate consumption used not for growth purposes if not for requiring of energy to repair damaged cellular components, to transfer nutrients and products in and out of cells, for motility, etc.

The lactate production was expressed as:

$$\frac{dC_{lac}}{dt} = Y_{PS} \cdot \text{Gluc consume} \quad (\text{A7})$$

Where Y_{PS} is the yield coefficient that means the amount of lactate produced per the amount of glucose consumed in kg lactate kg glucose⁻¹.

Finally, the O_2 nutrient was evaluated adapted the Michaelis-Menten kinetics comprising the oxygen transmission rate across the membrane (OTR) in kg O_2 m⁻² h⁻¹ representing the same as J_i in Eq. A3, the cellular oxygen consumption rate by cells (OUR)

in kg O₂ h⁻¹ (Eq. A8) and the mass balance in cellular chamber that differs from Eq. A4, (Eq. A9).

$$OTR = q_{oxygen} \cdot Cells\ number \cdot t \quad (A8)$$

$$Vol_{cell} \cdot \frac{dCoxygen_{cell}}{dt} = OTR \cdot Am - OUR \quad (A9)$$

Where q_{oxygen} is the metabolic consumption rate per cell in kg O₂ cell⁻¹ h⁻¹.

The amount of delivered oxygen is a significant factor in designing the cell culture bioreactors. For oxygen, furthermore, it was assumed that both the vascular chamber and feeding tank were in oxygen saturation conditions due to the use of silicone tubes that permitted the oxygenation with complete replenishment of the oxygen concentration. So, it was considered only variation of oxygen due to the cells consume.

3. Mass balances in the perfusion cell

The overall flowrate balance was done for the perfusion cell (Eq. A10):

$$Fi = Fp + Fr \quad (A10)$$

Being Fi the inlet flowrate pumping that was constant and Fr the recirculation flowrate that went from the vascular chamber of the perfusion cell to the feeding tank, both in m³ h⁻¹. The flow balance to calculate the value of Fp was defined as (Eq. A11):

$$Fp = K_{total} \cdot A_m \cdot \Delta P \quad (A11)$$

Being K_{total} the total permeability constant that changed with time because of fouling. It was defined as:

$$K_{total} = 1/(\mu \cdot (Rm + Rf)) \quad (A12)$$

With μ the viscosity of PBS at 37 °C. The permeance takes into account the sum of the resistances in the membrane. Rm is the resistance of the clean membrane and Rf makes mention to the cake layer model resistance. With the definition of Rf :

$$Rf = \alpha_f \cdot Cb \cdot \left(\frac{Vp}{Am} - Jss \cdot t \right) \quad (A13)$$

ΔP was directly measured by the pressure transducer and an average was done. J_{ss} was obtained representing the permeate flux versus time and seeing the data that corresponded to the steady state. R_m was obtained for each experiment at time = 0 with Eq. A14, A15:

$$Km = \frac{\Delta P}{J} \quad (A14)$$

$$R_m = \frac{1}{\mu \cdot Km} \quad (A15)$$

And doing an average between the different values. Finally, α_f was calculated graphically plotting R_f versus V_p , aiding with the Darcy's law to obtain R_f from the experimental data with Eq. A16:

$$Km = \frac{1}{\mu \cdot (R_m + R_f)} \quad (A16)$$

4. Mass balances in the feeding tank

The overall flowrate balance was done for the feeding tank. It was supposed two scenarios: not changes in volume (Eq. A17) or changes in a constant flowrate due to sampling (Eq. A18):

$$\frac{dV}{dt} = 0 \quad (A17)$$

$$\frac{dV}{dt} = (-V_{sample}) \quad (A18)$$

Being V_{sample} an apportionment calculated, fixing take 2 samples per day and both in the permeate and in the culture medium solution of 0.5 mL per sample in order to analyze the evolution of glucose cells consume and lactate production, and the concentration of BSA to evaluate the fouling.

The mass component balances were done (Eq. A19):

$$C_{i,t} \cdot \frac{dV}{dt} + V \cdot \frac{dC_{i,t}}{dt} = Fp \cdot C_{i,cell} + Fr \cdot C_{i,v} - Fi \cdot C_{i,t} - V_{sample} \cdot C_{i,t} \quad (A19)$$

Being $C_{i,t}$ the concentration of the i component in the culture medium tank in $kg\ m^{-3}$.

For not changes in volume the last term in Eq. A19 was neglected.

SIMPLIFIED MODEL DEVELOPMENT**1. Mass balances in the membrane**

The term of diffusion mass transport was neglected, converting Eq A3. in Eq. A20:

$$J_i = C_{i,v} \cdot K_{total} \cdot P \quad (A20)$$

At time = 0 the concentration of glucose in vascular chamber was 4.5 kg m⁻³ that is the concentration of glucose in the DMEM medium used since it is foreseen develop the tests in dynamic with this usual medium in TE for glioblastoma cells and the lactate concentration was 0 kg m⁻³ for the same reason.

2. Mass balances in the cellular chamber

The model remained equal for glucose and lactate components. At time = 0, the concentration of glucose and lactate were the same as in the vascular chamber.

For oxygen, Eq. A3 for oxygen was converted into Eq. A21:

$$J_i = (C_{oxygen,v} - C_{oxygen,cell}) \cdot \frac{D_{oxygen,cell}}{\Delta x_{cell}} \quad (A21)$$

The oxygen saturation concentration for vascular chamber was fixed in 0.00674 kg O₂ m⁻³ and at time = 0, the cellular chamber had the same concentration.

3. Mass balances in the perfusion cell

The equations for the perfusion cell were the same as in the complete model.

4. Mass balances in the feeding tank

The final scenario considered were the change of volume with sampling (Eq. A17 and A18). The initial concentration for glucose in the feeding was 4.5 kg m⁻³ and for lactate 0 kg m⁻³.

ASPEN CUSTOM MODELER V9

Using the ACM computational tool, the system (Figure 6.6) was modelled.

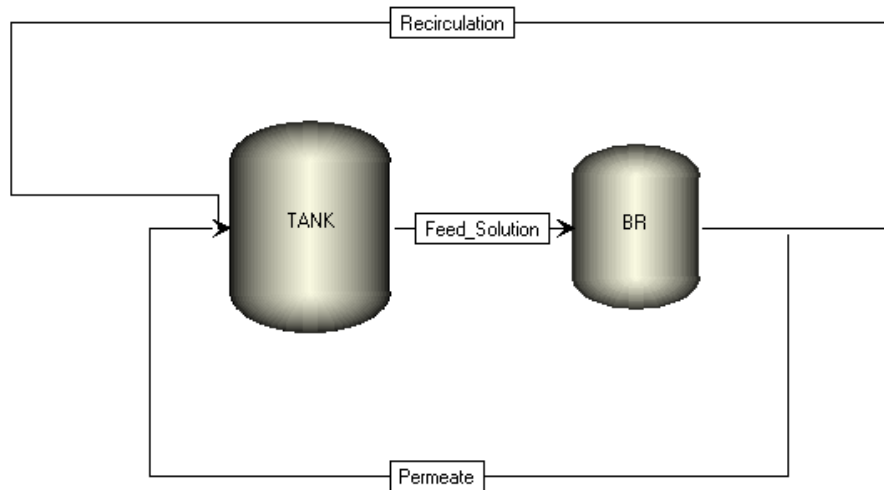


Figure 6. 6. ACM diagram for the perfusion BR system.

- a) Mathematical model for the combined pore blockage and cake filtration model for protein (BSA) during microfiltration

//Definition of current variables

Port Feed

Fi as RealParameter (6e-5); //Feed flowrate = m3/h (constant), 5.1e-5 for 48 rpm

End

Port Permeate

Fp as flow_vol; //Permeate flowrate = m3/h

End

Port Recirculation

Fr as flow_vol; //Recirculation flowrate m3/h

End

Model Perfusion_Cell

//Variables

```
Rm as notype; //Membrane resistance = m^-1

Rf as notype; //Fouling resistance = m^-1

alfa as notype(fixed,25.5651); //Pore blockage parameter = m^2/kg

beta as notype(fixed,2.4e12); //Specific protein layer resistance = m/kg

Rfo as notype(fixed,6.94e13); //Resistance of a single protein agreggate = m^-1

Cb as notype(fixed,0.4); //BSA concentration in the feed solution = kg/m3

Fpo as notype; //Initial flowrate = m^3/h

//Parameters

Km as RealParameter(1.022); //Permeance (clean membrane) = m^3/(m^2*h*bar)

P as RealParameter(0.022); //Working pressure = bar

Am as RealParameter(6.157e-4); //Scaffold area = m^2

visc as RealParameter(1.94e-12); //Viscosity of PBS at 37 °C = Bar*h

//Definition of inputs and outputs

inlet_f as input Feed; //Feed flow into the BR

outlet_r as output Recirculation; //Recirculation flow out of the BR

outlet_p as output Permeate; //Permeate flow out of the BR

//Equations

inlet_f.Fi=outlet_r.Fr+outlet_p.Fp;

outlet_p.Fp=Fpo*(exp(-alfa*P*Cb*time/visc/Rm)+(Rm/(Rm+Rf))*(1-exp(-
alfa*P*Cb*time/visc/Rm))));

Rm=1/visc/Km;

Fpo=P*Am/visc/Rm;
```

```
Rf=(Rm+Rfo)*sqrt(1+(2*beta*P*Cb*time/(visc*(Rm+Rfo)^2)))-Rm;
```

```
End
```

```
Model Tank
```

```
//Variables
```

```
V as volume; //Volume = m^3
```

```
//Definition of inputs and outputs
```

```
inlet_r as input Recirculation; //Recirculation flow into the tank
```

```
inlet_p as input Permeate; //Permeate flow into the tank
```

```
outlet_f as output Feed; //Flow out of the tank
```

```
//Equations
```

```
$V=0;
```

```
End
```

b) Mathematical model for cellular analysis

```
//Definition of current variables
```

```
Port Feed
```

```
Cglu as conc_mass; //Concentration of glucose = kg/m3
```

```
Clac as conc_mass; //Concentration of lactate = kg/m3
```

```
Fi as RealParameter (6e-5); //Feed flowrate = m3/h, 5.1e-5 for 48 rpm
```

```
End
```

```
Port Permeate
```

Cglu as conc_mass; //Concentration of glucose = kg/m³

Clac as conc_mass; //Concentration of lactate = kg/m³

Fp as flow_vol; //Permeate flowrate = m³/h

End

Port Recirculation

Cglu as conc_mass; //Concentration of glucose = kg/m³

Clac as conc_mass; //Concentration of lactate = kg/m³

Fr as flow_vol; //Recirculation flowrate m³/h

End

Model Perfusion_cell

//Variables

Jglucose as notype; //Permeate flux of glucose = kg glucose/(m²*h)

Cglucosev as conc_mass; //Concentration of glucose in vascular chamber = kg
glucose/m³

Cglucosecell as conc_mass; //Concentration of glucose in cellular chamber = kg
glucose/m³

Jlactate as notype; //Permeate flux of lactate = kg lactate/(m²*h)

Clactatev as conc_mass; //Concentration of lactate in vascular chamber = kg
lactate/m³

Clactatecell as conc_mass; //Concentration of lactate in cellular chamber = kg
lactate/m³

numbercell as constant; //Number of cells produced per time = cells/h

```
glucoseconsume as notype; //Glucose consumed by cells = kg glucose/h

lactateproduction as notype; //Lactate produced by cells = kg lactate/h

OTR as notype; //Oxygen transmission rate = kg O2/(m^2*h)

OUR as notype; //Cellular oxygen consumption rate = kg O2/h

Coxygenv as conc_mass; //Oxygen concentration in vascular chamber = kg O2/m^3

Coxygencell as conc_mass; //Oxygen concentration in culture media = kg O2/m^3

Ktotal as notype; //Total permeability constant = m^3/(m^2*h*bar)

Rf as notype; //Cake layer resistance = m^-1

//Fixed parameters

Rm as RealParameter(2.66e11); //Membrane resistance = m^-1

P as RealParameter(0.022); //Working pressure = bar

alfa as RealParameter(1.67e14); //Intrinsic resistance of the cake layer = m/kg

Cbsa as RealParameter(0.4); //BSA concentration in the feed solution = kg/m3

Jss as RealParameter(2.20e-6); //Permeate flux at steady state conditions = m^3/h

visc as RealParameter(1.94e-12); //Viscosity of PBS at physiological temperature =
Bar*h

Volvascular as RealParameter(2.77e-6); //Volume of vascular chamber = m^3

Volcell as RealParameter(5.54e-6); //Volume of cellular chamber = m^3

Am as RealParameter(6.157e-4); //Scaffold area = m^2

Doxygencell as RealParameter(5.76e-6); //Diffusion coefficient for neuronal tissues
across the cell layer = m^2/h

qoxygen as RealParameter(8.87e-14); //Oxygen consumption rate for neurons = kg
O2/(cell*h)

m as RealParameter(0.57); // Maintenance coefficient = kg glucose/(h*kg cells)
```



```
masscell as RealParameter (27e-15); //Mass of one cell = kg/cell

Yxs as RealParameter(0.013); //Yield coefficient cells/glucose = kg cells/kg glucose

Yps as RealParameter (0.73); //Yield coefficient lactate/glucose = kg lactate/kg glucose

xcell as RealParameter(10e-9); //Outer membrane of nerve cells thickness = m

//Definition of inputs and outputs

inlet_f as input Feed; //Feed flow into the BR

outlet_r as output Recirculation; //Recirculation flow out of the BR

outlet_p as output Permeate; //Permeate flow out of the BR

//Current connections

inlet_f.Cglu=Cglucosev;

outlet_r.Cglu=Cglucosev;

outlet_p.Cglu=Cglucosecell;

inlet_f.Clac=Clactatev;

outlet_r.Clac=Clactatev;

outlet_p.Clac=Clactatecell;

//Equations

//NUTRIENT BALANCE: GLUCOSE

Jglucose=Cglucosev*Ktotal*P; Volcell*$Cglucosecell=Jglucose*Am-
outlet_p.Fp*Cglucosecell-glucoseconsume;

//METABOLITE BALANCE: LACTATE
```

```
Jlactate=Clactatev*Ktotal*P; Volcell*$Clactatecell=Jlactate*Am-  
outlet_p.Fp*Clactatecell+lactateproduction;
```

```
//NUTRIENT BALANCE: OXYGEN
```

```
OTR=(Coxygenv-Coxygencell)*Doxygencell/xcell;
```

```
OUR=qoxygen*numbercell*time;
```

```
Volcell*$Coxygencell=OTR*Am-OUR;
```

```
//CELLS
```

```
numbercell=-14.12*time^2+4919.4*time+57000;
```

```
glucoseconsume=numbercell*masscell*(1/Yxs+m*time);
```

```
lactateproduction=Yps*glucoseconsume;
```

```
//BIOREACTOR
```

```
inlet_f.Fi=outlet_r.Fr+outlet_p.Fp; //Flowrate balance = m^3/h
```

```
Ktotal*P*Am=outlet_p.Fp; //Permeate flow balance = m^3/h
```

```
Ktotal=1/(visc*(Rm+Rf)); //Variation of permeability constant due to resistances =  
m^3/(m^2*h*bar)
```

```
Rf=alfa*Cbsa*time*(outlet_p.Fp-Jss)/Am; //Fouling resistance variation = m^-1
```

```
End
```

```
Model Tank
```

```
//Variables
```

```
V as volume; //Volume = m3
```

```
Vsample as flow_vol; //Volume of sample taken per time = m3/h
```

Cglucoset as conc_mass; //Variable concentration of glucose in the tank = kg/m3

Clactatet as conc_mass; //Variable concentration of lactate in the tank = kg/m3

//Definition of inputs and outputs

inlet_r as input Recirculation; //Recirculation flow into the tank

inlet_p as input Permeate; //Permeate flow into the tank

outlet_f as output Feed; //Flow out of the tank

//Current connections

outlet_f.Cglu=Cglucoset;

outlet_f.Clac=Clactatet;

//Equations

\$V=(-Vsample);

Cglucoset*\$V+V*\$Cglucoset=inlet_p.Fp*inlet_p.Cglu+inlet_r.Fr*inlet_r.Cglu-

outlet_f.Fi*Cglucoset-Vsample*Cglucoset;

Clactatet*\$V+V*\$Clactatet=inlet_p.Fp*inlet_p.Clac+inlet_r.Fr*inlet_r.Clac-

outlet_f.Fi*Clactatet-Vsample*Clactatet;

End

Appendix F: Glucose diffusivity results

Based on Fick's first Law, due to the concentration gradient, glucose went from the glucose compartment to the water compartment and this diffusion flux was calculated as (Eq. A22):

$$J = \frac{\text{Total mass of glucose}}{A \cdot t} \quad (\text{A22})$$

Knowing the membrane area (A_m) in m^2 , the total mass of glucose in grams and the experiment time (t) in hours.

The total mass of glucose was calculated with the concentrations obtained and taking into account the changes in volume in the diffusion cell because of the samples taken. It was checked that the total mass of glucose (Eq. A23) remained constant in all experimental points:

Total mass of glucose =

$$C_{gluc-gluc\ compartment} \cdot V_{gluc\ compartment} + C_{gluc-water\ compartment} \cdot V_{water\ compartment} \quad (A23)$$

With the glucose diffusion flux, the gradient concentration between both compartments and knowing the thickness of the membrane, the glucose diffusion coefficient can be calculated (Eq. A24):

$$D_{gluc} = \frac{J_{gluc}}{\Delta C} \cdot \delta \quad (A24)$$

Table 6.1 shows the results for experiments done to calculate the glucose effective diffusivity. The volume of glucose and water compartments was recalculated measuring the final volume and taking into account the sample volume taken and the volume removed by evaporation.

The effective diffusivity was determined by fitting the experimental data, representing the diffusion flux of glucose versus the concentration gradient of both compartments and obtaining the slope of the graph, with the 100 μm of thickness.

Table 6. 1. Average data for glucose diffusivity experiments

Time (h)	Glucose 5g/L (cm^3)	UP Water (cm^3)	$\overline{\Delta C}$ (g/m^3)	$\overline{\Delta J_{gluc}}$ (g/m^2s)
0	280.0	280.0	4744.18	-
3	277.5	277.5	3331.57	0.0796
22	275.0	275.0	2372.70	0.0108
46	272.5	272.5	1204.16	0.0053
70	270.0	270.0	959.55	0.0034
142	264.9	264.9	716.60	0.0017

Figure 6.7 represents the variation of the concentration gradient with time.

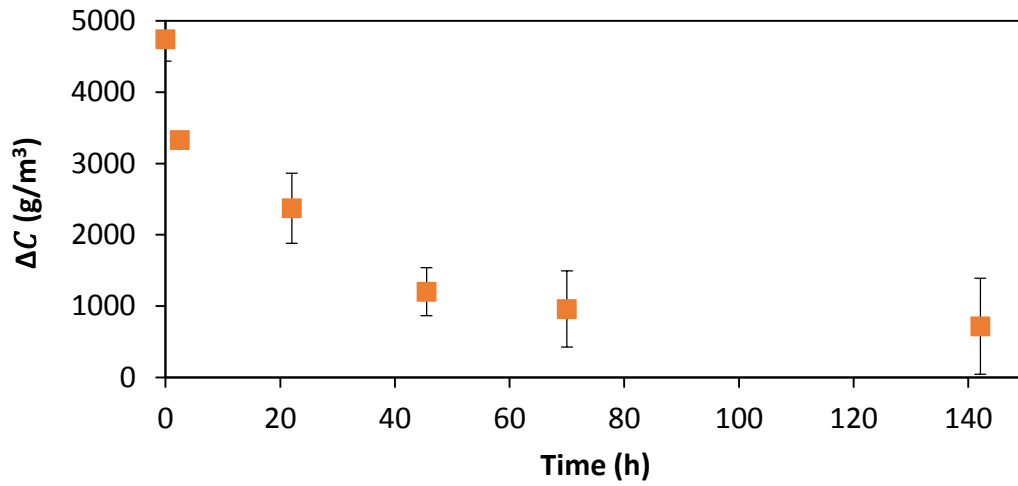


Figure 6. 7. Variation of the concentration gradient with time

Figure 6.8 shows the diffusion flux versus the concentration gradient to obtain a fixed slope fitting the representation to a line. The slope is equal to the $D_{\text{Gluc,eff}}$ divided to the thickness of the membrane.

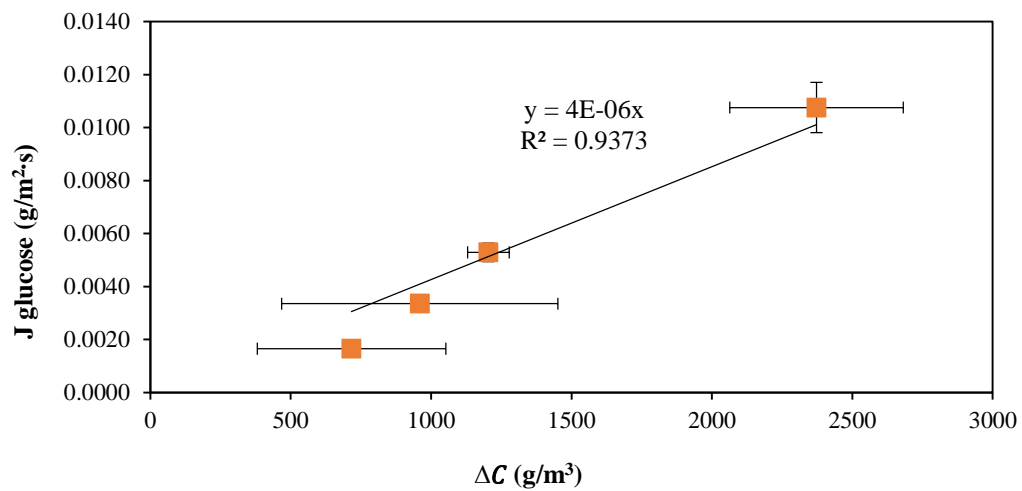


Figure 6. 8. Glucose diffusion flux versus concentration gradient

Appendix G: Continuous and discrete measurements of oxygen

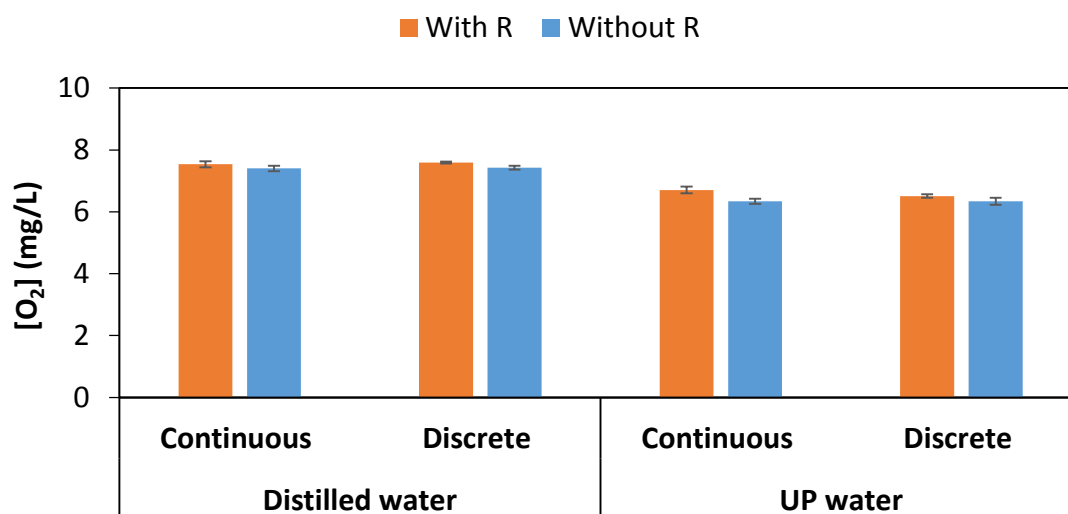


Figure 6. 9. Oxygen concentration with and without recirculation, for continuous and discrete measurements in water

Appendix H: Reynolds number calculation

For the case of the non-circular system, the Re number is expressed as:

$$N_{RE} = 4r_H\bar{V}\rho/\mu \quad (\text{A27})$$

With r_H the hydraulic radio that was calculated as:

$$r_H = S/L_P \quad (\text{A28})$$

Where L_p is the perimeter of the perfusion cell. The parameters considered are collected in Table 6.2.

Table 6. 2. Data for calculated the Re number in the perfusion cell.

Parameters	Values	Units
ρ	993.37	kg m^{-3}
μ	$6.92 \cdot 10^{-4}$	Pa s
\bar{V}	$1.32 \cdot 10^{-4}$ and $1.12 \cdot 10^{-3}$	m s^{-1}
r_H	$1.94 \cdot 10^{-3}$	m
L_P	$6.50 \cdot 10^{-2}$	m
S	$1.26 \cdot 10^{-4}$	m^2

A Re number of 1.47 was obtained for 1 mL/min and a Re of 12.5 at 8.5 mL/min.

Appendix I: Cells growth kinetic parameters

A sensitivity analysis was made for the important parameters of the cell growth equations (Monod parameters). A range of measurement between the values found in literature was evaluated.

The value of the maintenance coefficient is specific for each cell type and depends on the type of substrate consumed and on environmental conditions such as pH and temperature. For that, it was observed that the higher this coefficient was, higher glucose was consumed by cells (Figure 6. 10). This is due to the fact that a higher maintenance coefficient, higher quantity of glucose the cells needed to alive. In the more restrictive case, when $m = 0.934$, it is observed that glucose was completely consumed. While with a coefficient $m = 0.4$ after 5 days, 1.18 kg of glucose m^{-3} remained.

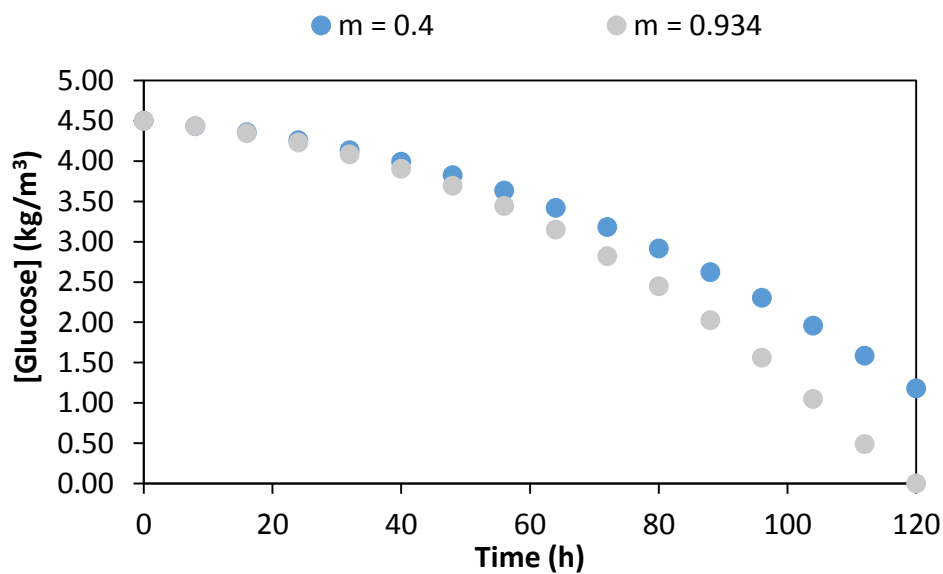


Figure 6. 10. Variation of glucose concentration with time depending on the maintenance coefficient.

The consumption of glucose is directly related to the production of lactate (metabolic product). Therefore, with a higher maintenance coefficient, higher production of lactate (Figure 6. 11). The rest of the main variables did not change with the change in m .

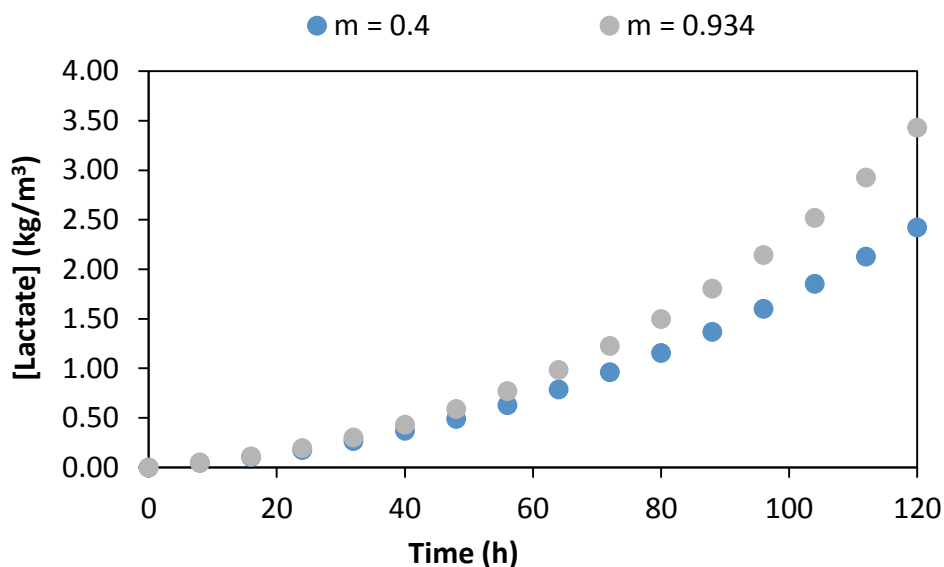


Figure 6. 11. Variation of lactate concentration with time depending on the maintenance coefficient.

For yield coefficients it has been verified that a high value of Y_{ps} supposed a higher production of lactate in relation to the glucose consumed but did not produce any change in the rest of the variables of the system (Figure 6.12).

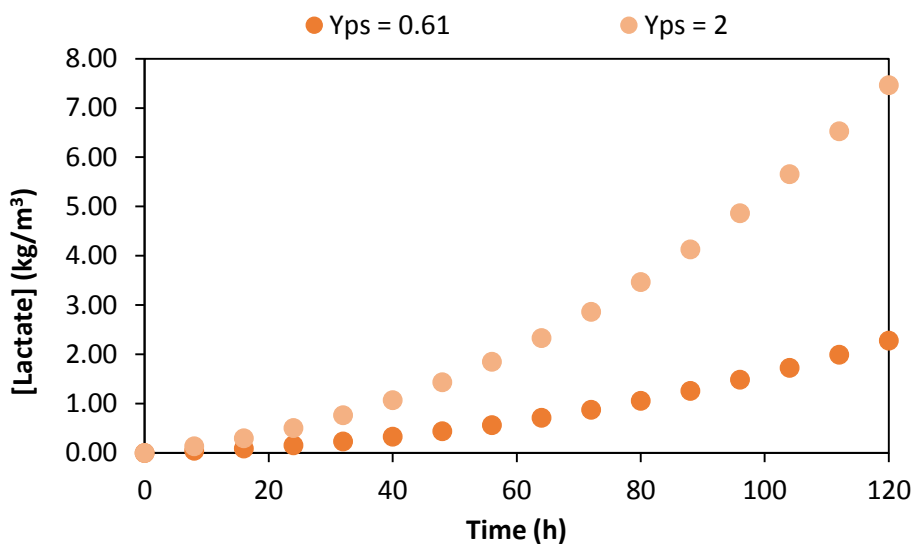


Figure 6. 12. Variation of lactate concentration with time depending on the Y_{ps} yield coefficient.

Y_{xs} yield coefficient describes the relationship between cells and glucose consume. A lower coefficient means that more glucose the cells need. In Figure 6.13 and 6.14 it could be seen that a $Y_{xs} = 0.01$ is much restrictive than the other $Y_{xs} = 0.03$. With the first one, at 120 h the glucose was totally consumed, whereas with the other yield value, 2 kg glucose m^{-3} were in the cellular chamber.

In the lactate production the difference between both yield produced a duplication in the concentration of lactate in cellular chamber, being in the limit of danger for cells in the case of $Y_{xs} = 0.01$.

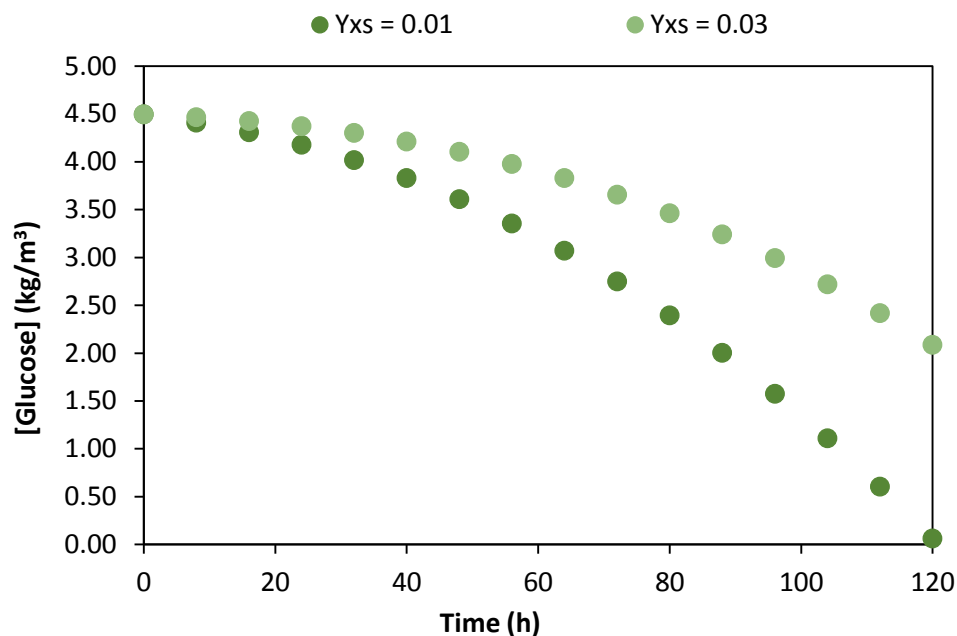


Figure 6.13. Variation of glucose concentration with time depending on the Y_{xs} yield coefficient.

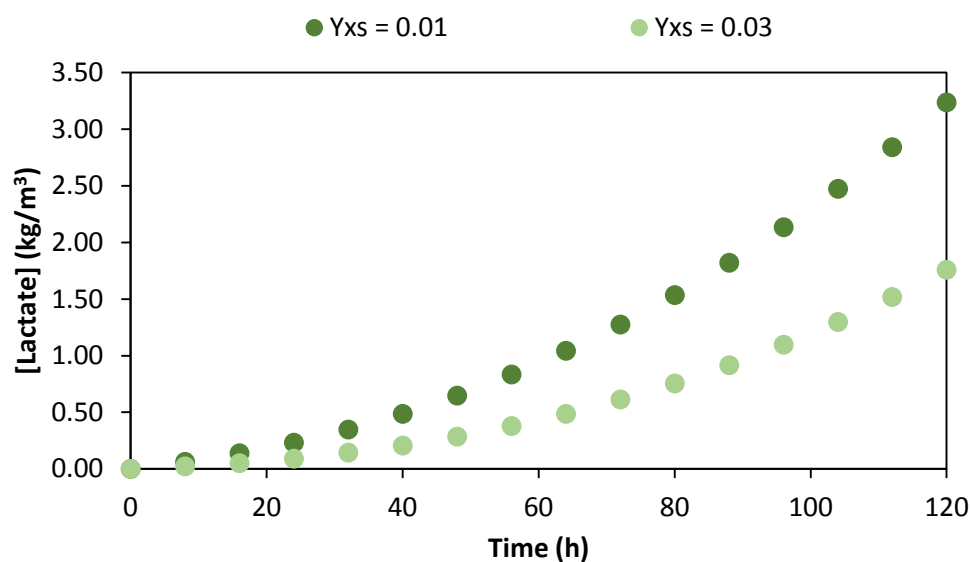


Figure 6.14. Variation of lactate concentration with time depending on the Y_{xs} yield coefficient.

The yield and maintenance coefficients have a great importance in the system, varying with the cell type. With this, the necessity of carrying out a planning of experiments for its obtaining is confirmed. Also, as a preliminary study, it was useful to see the behavior of the cellular systems referenced for the bioreactor perfusion system.